Quaternary Science Reviews 322 (2023) 108384

Contents lists available at ScienceDirect

Quaternary Science Reviews

journal homepage: www.elsevier.com/locate/quascirev

The aggradation of alluvial fans in response to monsoon variability over the last 400 ka in the Hajar Mountains, south-east Arabia

Sam Woor [a,*], David S.G. Thomas [a,b], Julie A. Durcan [a], Sallie L. Burrough [a], Ash Parton [c,d]

[a] School of Geography and the Environment, University of Oxford, Oxford, UK
[b] Geography, Archaeology & Environmental Studies, University of the Witwatersrand, Johannesburg, South Africa
[c] Human Origins and Palaeoenvironments Research Group, Oxford Brookes University, Oxford, UK
[d] Mansfield College, University of Oxford, Oxford, UK

ARTICLE INFO

Handling Editor: Claudio Latorre

Keywords:
Climate change
Indian ocean monsoon
Luminescence dating
palaeoenvironments
Geomorphology
Arabia

ABSTRACT

The preservation and interpretation of past external forcings within sedimentary archives can be complicated. Marine proxy records show that, throughout the Mid-Late Quaternary, monsoon rainfall in south-east Arabia has varied at precessional timescales (~ 23 ka). By contrast, terrestrial environmental records from the region, such as speleothems and palaeolake sequences, generally only capture rainfall variability at eccentricity (~ 100 ka) timescales and geomorphological archives rarely record events over multiple glacial cycles. Previous work has suggested that the alluvial fan systems of the Hajar Mountains record aggradation coincident with precessional peaks because of more northerly Indian Ocean Summer Monsoon (IOSM) rainfall, relative to present. However, the alluvial record is complex: there is a growing body of 'anomalous' aggradation age data from periods of precessional minima and it is spatially uneven, mainly being derived from fans at either the northern- or southern-most extents of the western side of the mountains.

We present optically stimulated luminescence (OSL) ages of alluvial aggradation from new sites in the central portion of the western and eastern sides of the Hajar mountains. Sedimentary units that show evidence of more sustained flow conditions, such as coarse conglomerate deposition and the development of thick floodplain deposits, typically date to periods of higher IOSM rainfall at precessional timescales. Sites where there is evidence of deposition under more ephemeral flow conditions, like today, yield ages corresponding to precessional minima. We synthesise these data with similarly interpreted alluvial and lacustrine deposits from across the region, employing a hierarchical clustering approach to generate clusters of ages representing periods of increased hydrological activity. This objective approach to regional chronological data suggests that ten periods of more sustained hydrological activity are evidenced across the Hajar region, broadly aligning to precessional and eccentricity peaks over the last 400 ka. These clusters show that Hajar fans predominately aggrade because of increasing rainfall over their catchments, with the central ages of clusters often aligning with the onset of precessional forcing. Hajar alluvial systems preserve important records of Quaternary climate variability over long timescales in an arid region where terrestrial records are scarce due to preservation issues.

1. Introduction

Today, south-east Arabia is characterised by an arid to hyper-arid climate, with the northerly extent of Indian Ocean Summer Monsoon (IOSM) rainfall only reaching the southern coast of Arabia (Fig. 1). However, South-east Arabia has experienced considerable palaeoclimatic and palaeoenvironmental variability through the Late Quaternary. Marine sediment cores from the Arabian Sea (e.g. Sirocko et al., 1993; Overpeck et al., 1996; Clemens and Prell, 2003; Ziegler et al., 2010; Caley et al., 2011) and speleothem records from the Hajar Mountains (e.g. Fleitmann et al., 2003; Burns et al., 2001; Burns et al., 1998) show that the periodic northwards displacement and intensification of the IOSM resulted in periods of higher rainfall in south-east Arabia (Fig. 1). Inferences from palaeoclimate archives are further supported by modelling studies that show higher rainfall over south-east Arabia periodically during the last 130 ka (Jennings et al., 2015). These

* Corresponding author.
E-mail addresses: samuel.woor@ouce.ox.ac.uk (S. Woor), david.thomas@ouce.ox.ac.uk (D.S.G. Thomas), julie.durcan@ouce.ox.ac.uk (J.A. Durcan), sallie.burrough@ouce.ox.ac.uk (S.L. Burrough), ash.parton@mansfield.ox.ac.uk (A. Parton).

https://doi.org/10.1016/j.quascirev.2023.108384
Received 24 June 2023; Received in revised form 23 October 2023; Accepted 26 October 2023
Available online 11 November 2023

periodic incursions of the IOSM are driven by increases in insolation oscillating at precessional (~ 23 ka) timescales (Parton et al., 2015a).

These palaeoclimate archives offer a regional signal of Quaternary precipitation variability. However, establishing landscape-scale responses to climate change is an important challenge for understanding their sensitivity to external forcing and what climatic signals are preserved in sedimentary archives (Whittaker, 2012; D'Arcy and Whittaker, 2014). This challenge requires proxy data from landforms. Geomorphological records of environmental change, termed geoproxies (Thomas and Burrough, 2012), offer a means for understanding landscape responses to both regional-scale climatic drivers and smaller-scale controls throughout the Late Quaternary (Thomas, 2013). Whilst the number of luminescence or radiocarbon-dated sedimentary records from landforms in south-east Arabia has grown considerably over the last 20 years (Woor et al., 2022a), arid regions often lack geoproxy records that preserve landscape responses to external forcing over multiple glacial cycles due to the limited preservation potential of features such as lake beds during intense arid phases (Thomas, 2013).

1.1. The IOSM model of precessionally-paced alluvial fan aggradation in the hajar

The Hajar Mountains, which run from northern Oman to the Musandam Peninsula in the northern UAE, have extensive alluvial deposits, forming valley-fill sequences within mountain catchments and large fans which extend both to the Arabian Sea and the interior Rub'al Khali desert (Woor et al., 2023). The classic model of dryland fan response to Quaternary climatic variability is that they aggrade during periods of higher rainfall as sediment supply increases from their catchments, juxtaposed with becoming net incisional during periods of greater aridity when sediment supply decreases leading to incision and the abandonment of relict surfaces (Lecce, 1990; Blair and McPherson, 1994; Harvey, 2011). The response of fans to climatic change does, however, vary somewhat depending on the specific contexts of their feeding catchments (Blair and McPherson, 1994). This means that fans can hold important information about the nature of the response of sediment routing from upland source areas to down-system sinks to

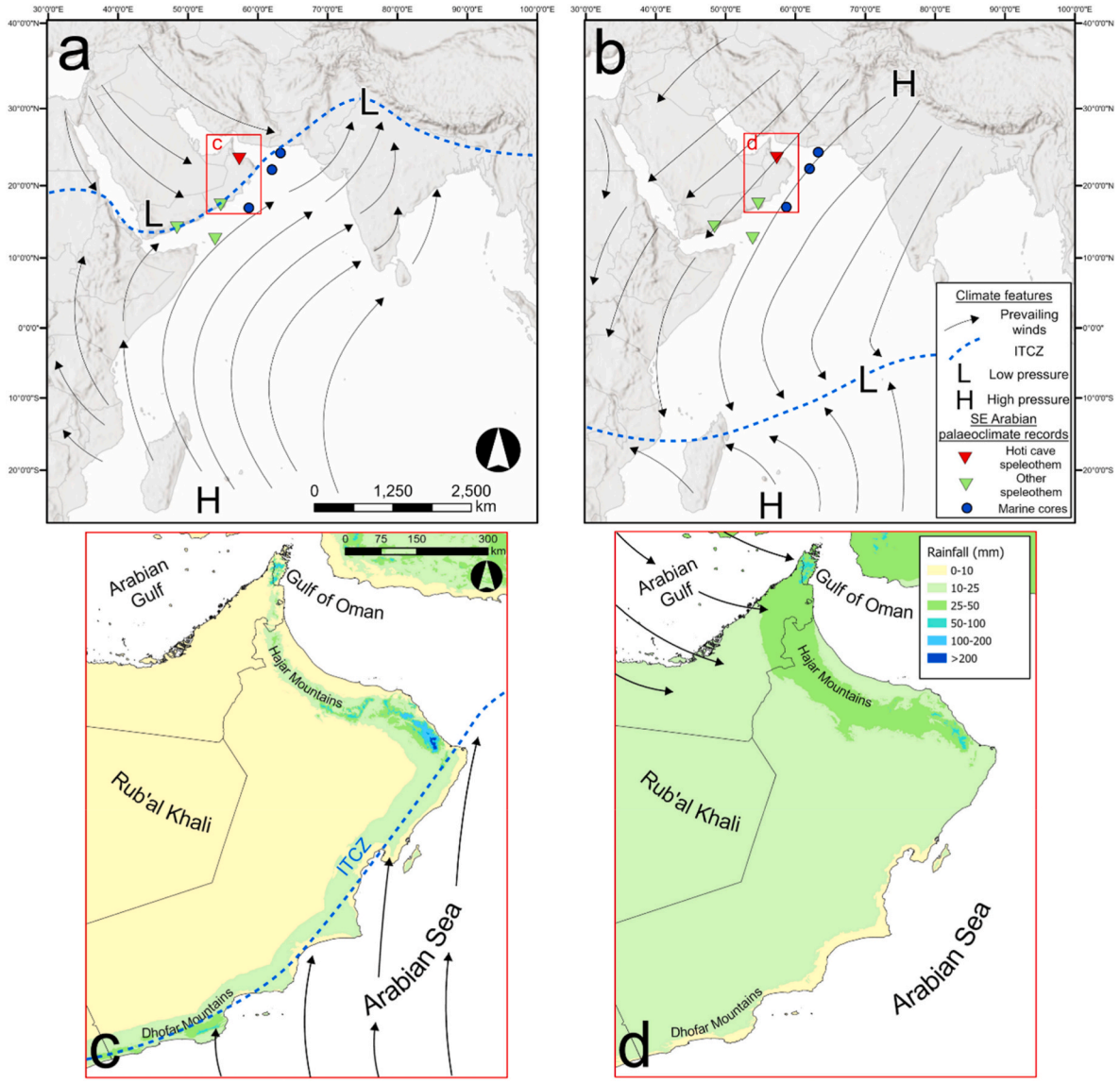

Fig. 1. **(a)** The circulation of the Indian Ocean Monsoon system and the position of the inter-tropical convergence zone (ITCZ) during summer months. **(b)** The circulation of the Indian Ocean Monsoon system and position of the ITCZ during winter months. Key palaeoclimate records are shown, including the Hoti Cave, located in the Hajar Mountains. Redrawn from Fleitmann and Matter (2009). The red boxes indicate the extent of south-east Arabia, shown in **(c)** and **(d)**. **(c)** Mean rainfall in south-east Arabia during summer months (June–August). **(d)** Mean rainfall in south-east Arabia during winter months (January–March). Rainfall data for 1970–2000 from WorldClim 2 (Fick and Hijmans, 2017).

climate forcing (Savi et al., 2020). Indeed, fans in low-latitude desert environments have been shown to record cycles of aggradation and incision that are paced by orbital-scale climate forcing (e.g. D'Arcy et al., 2017; Terrizzano et al., 2017; Schildgen et al., 2019; Bartz et al., 2020).

To date, fan paleoenvironmental analyses in the Hajar have focused on the fans of the eastern UAE and the large megafans in central Oman, which are both located on the western flanks of the Hajar Mountains. Luminescence and radiocarbon ages record periods of sediment deposition under more sustained channel flow conditions, in-sync with precessionally-paced periods of IOSM intensification (e.g. Blechschmidt et al., 2009; Atkinson et al., 2013; Parton et al., 2013, 2015b; Mueller et al., 2022). This conforms to the general model of sediment aggradation during wetter periods for dryland fans, and also corresponds with higher monsoon rainfall intensity recorded in marine core records (Clemens and Prell, 2003). As such, the model established in the literature is one of precessionally-paced Hajar fan aggradation in response to higher rainfall from a more northerly, intensified IOSM. This has been exemplified by the Al Sibetah site in the UAE, showing the aggradation of coarse fan conglomerates across multiple precessional cycles from ~ 160-55 ka (Parton et al., 2015a). Herein, we refer to this response by Hajar fans to external climate forcing as the 'IOSM model'.

Many of these dated periods of hydrological intensification and aggradation in alluvial systems as a result of increased sediment supply are supported by other environmental records from the region, such as the Hoti Cave speleothem isotopic record from the central Hajar (e.g.

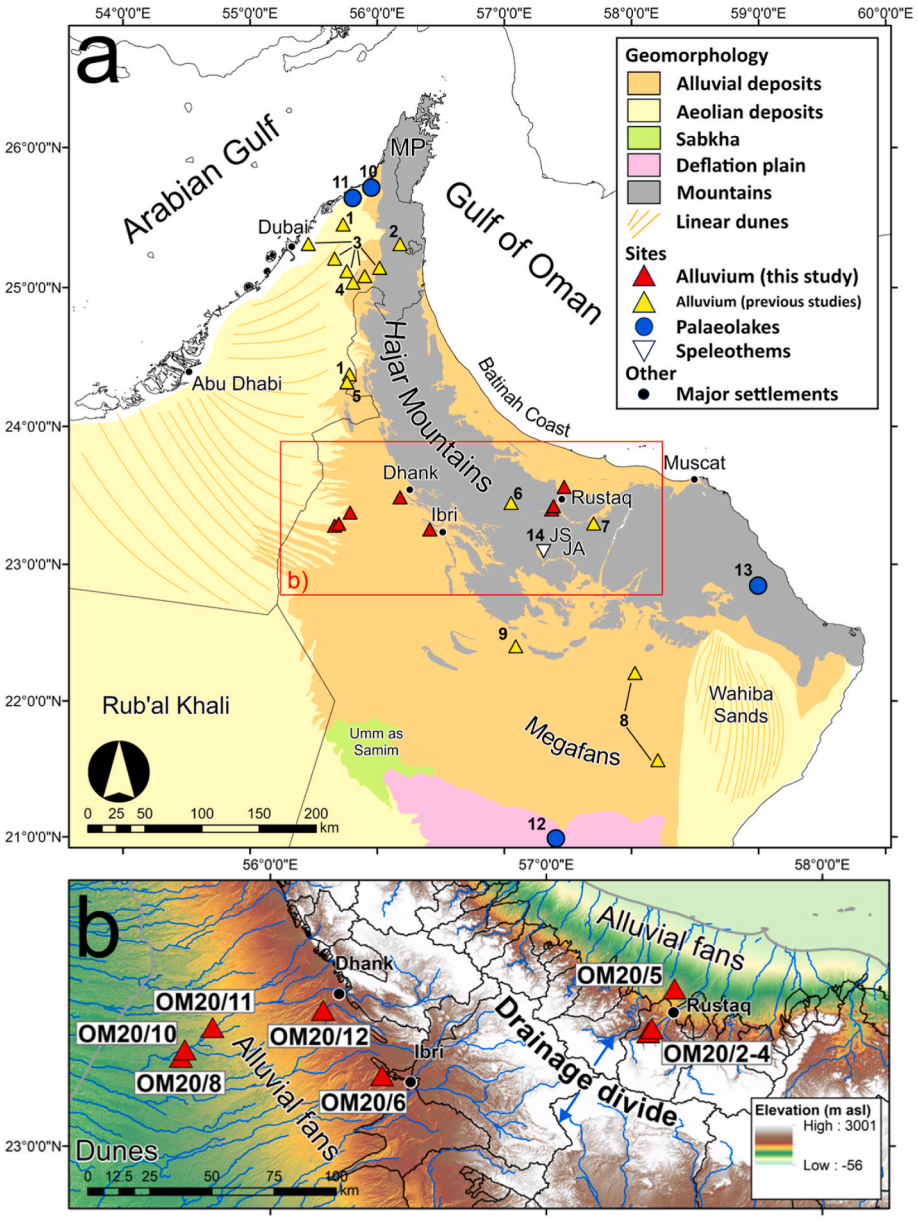

Fig. 2. **(a)** The Hajar Mountains of northern Oman and the north-eastern UAE showing regional geomorphological features and key sites with previously dated alluvium using OSL and radiocarbon: 1: Atkinson et al. (2013), 2: Purdue et al. (2019), 3: Mueller et al. (2022), 4: Parton et al. (2013), 5: Parton et al. (2015a), 6: Moraetis et al. (2020), 7: Hoffmann et al. (2015), 8: Blechschmidt et al. (2009) and 9: Beuzen-Waller et al. (2022). Other regional palaeoenvironmental sites are shown, including palaeolake deposits from: 10: Parker et al. (2006), 11: Preston et al. (2015), 12: Rosenberg et al. (2012) and 13: Fuchs and Buerkert (2008), as well as 14: the Hoti Cave speleothem (Burns et al., 2001). 'JA' denotes Jebel Ahkdar and 'JS' Jebel Shams. 'MP' denotes the Musandam Peninsula. **(b)** The study sites both east (OM20/3–5) and west (OM20/6–12) of the Hajar drainage divide. Sites OM20/3–4 are valley-fill deposits along Wadi Sahtan in the lower reaches of the mountain catchment feeding the Rustaq fan. Sites OM20/5–12 are alluvial fan deposits. Major drainage networks and mountain catchments are delineated by the blue and black lines, respectively.

Fleitmann et al., 2003) (Fig. 2). The speleothem record does not, however, record all the wetter phases represented in fan aggradation and marine core records. For example no growth is recorded during Marine Isotope Stage 3 (MIS 3; 60–30 ka) at Hoti Cave (Fleitmann et al., 2003). By contrast, multiple examples of alluvial aggradation from the region date to this period (e.g. Farrant et al., 2012; Parton et al., 2013; Mueller et al., 2022). It has also been demonstrated that Hajar alluvium can be dated using luminescence techniques back to as much as 900 ka in some circumstances, presenting old records of landscape change that are unprecedented in the region (Blechschmidt et al., 2009). These very old ages have been related to higher IOSM rainfall during peak interglacial conditions, although it is worth noting that they have large associated uncertainties almost spanning entire glacial cycles either side of the central age.

Despite the literature from the region consistently supporting the IOSM model at the *site scale*, the growing body of age data from Hajar fan systems is noisy and it is difficult to determine discrete periods of aggradation in line with precessional forcing at the *regional scale* using qualitative comparisons between records alone. Further, previous fan investigations have focused on the northern interior Hajar bajada in the UAE (e.g. Farrant et al., 2012; Parton et al., 2013, 2015a; Mueller et al., 2022) and the large megafans (with areas 10^3–10^5 km^2; Hartley et al., 2010) of the southern Hajar bajada (Blechschmidt et al., 2009). Fans along the Batinah Coastal plain east of the Hajar, the interior central bajada and valley-fill sequences within their mountain source areas have received limited or no palaeoenvironmental analysis compared to those described above (Fig. 2). The MIS 3 chronology presented by Hoffmann et al. (2015) for Wadi (Arabic term for an ephemeral channel) Mistal remains the only study of alluvial aggradation for an alluvial system draining east of the Hajar drainage divide to the Batinah Coast.

There is also a growing body of age data from alluvial sediments around the Hajar which appear at odds with the regional IOSM model. Beuzen-Waller et al. (2022) date deposition in Wadi Dishah, located at the mountain front of the southern Hajar, to 26.6 ± 1.8 ka, falling within MIS 2, a dry phase in the IOSM model during which aggradation is not expected. The Maqta Oasis, located in the central Hajar, records continuous, gradual deposition within a wetland environment throughout the arid Last Glacial Maximum and Terminal Pleistocene (20–12 ka) (Fuchs and Buerkert, 2008). Similarly, numerous aggradation events are recorded in alluvial fans along the interior mountain front of the UAE from 20–16 ka and again during the arid Late Holocene (3.5–1.6 ka; Mueller et al., 2022). These age data come from sedimentary units which are interpreted by the original authors as indicative of more ephemeral streamflow conditions. This suggests that careful sedimentary interpretation, as well as considerations of sampling location within large alluvial systems, are important for making climatic inferences in these contexts. Gathering data from areas of the Hajar for which no prior studies have been undertaken can, therefore, provide a means for testing these ideas.

1.2. Aims of this study

In this paper, we aim to test the hypothesis of IOSM-driven alluvial aggradation for fans in the central interior and eastern Hajar. To do this, we investigate, through field sedimentological interpretations and luminescence dating, new sites preserving Late Quaternary alluvial aggradation from mountain-front fan and valley-fill settings both west and east of the central Hajar Mountains. We also aim to more objectively define when periods of fan aggradation occurred across the Hajar region to test whether these periods align with precessional forcing. So, our new data are compiled with published sedimentary archives from alluvial and lacustrine settings across the Hajar. We employ hierarchical clustering to identify periods of aggradation in these systems and compare the results with palaeoclimate data from the Hoti Cave speleothem and marine cores from the Arabian Sea.

2. Regional setting

2.1. Regional geological and geomorphological setting

The Hajar Mountains developed through the collision of the Arabian Plate with the Eurasian Plate at the Makran subduction zone located in the Arabian Sea (Kusky et al., 2005) (Fig. 2). This process resulted in the Late Cretaceous uplift and exposure of the Semail ophiolite (ancient oceanic crust) which is the predominant geological unit of the Hajar Mountains (Guilmette et al., 2018). Uplift has continued throughout the Late Quaternary Period, although tectonic processes are spatially variable. Raised shorelines and faulting reported from the southern Hajar region indicate uplift of 100 m during the Pliocene and Quaternary (Kusky et al., 2005; Hoffmann et al., 2020), whereas the Musandam Peninsula at the northern tip of the Hajar range has experienced subsidence over this period (Ali et al., 2018). The highest peaks, Jebel Ahkdar and Jebel Shams, stand at around 3000 m asl and are located in the central Hajar (Fig. 2a).

Alluvial fans flank the fronts of the Hajar Mountains, ranging from small (10^{-3}-10^1 km^2), steep debris-flow dominated features in the northern Musandam Peninsula to large (up to 10^4 km^2), low gradient megafans in the southern Hajar (Fig. 2) (Woor et al., 2023). These large fans coalesce into bajadas (low-gradient alluvial plains) in the continental interior, as well as along the Batinah Coast parallel to the Arabian Sea. These two principle bajadas are fed by drainage from mountain catchments, the direction of which is controlled by the watershed which runs along the spine of the Hajar (Fig. 2b). These large fans typically display trenching by ephemeral stream systems (or *wadis*) at their apexes which extend down-fan to a distal intersection point. Here, they switch from being incisional to depositional, resulting in their telescopic progradation (Al-Farraj and Harvey, 2005). The larger megafans of the central and southern interior bajadas also preserve extensive networks of inverted palaeochannel networks which have been exhumed by aeolian deflation and more recent periods of flow (Maizels, 1987, 1990; Maizels and McBean, 1990). Extensive, rock varnished desert pavements mantle relict fan surfaces (Abrams and Chadwick, 1994; Al-Farraj and Harvey, 2000).

Many surfaces have been deeply incised by gullies formed by more recent flash flows under the presently arid climate. These events occur intermittently, with the largest flash floods commonly generated by tropical cyclones making landfall on the Batinah Coast, such as cyclone Shaheen in October 2021 (Terry et al., 2022). Events such as these as well as smaller-magnitude rainstorms have been observed to result in sediment reworking and deposition down-fan of sheet-like deposits of sand, although larger grain sizes are transported in the highest-magnitude flash floods such as those caused by the cyclones that occasionally hit the Batinah Coast (e.g. Kwarteng et al., 2009; Blechschmidt et al., 2009).

Whilst the fans of the Batinah Coast terminate in the Arabian Sea, the endorheic drainage systems which feed the large fans of the western interior terminate on the fringes of the Rub'al Khali. At the distal reaches of large megafans, numerous lacustrine basins have been reported, indicative of low-energy sinks (e.g. Rosenberg et al., 2012; Parker et al., 2016; Woor et al., 2023). Under the contemporary arid climate, these basins form sabkha such as the Umm as Samim (Fig. 2). In many distal locations, fan sediments have been over-topped by dune systems migrating eastwards from the Rub'al Khali since the Mid Holocene (Al Farraj and Harvey, 2004; Atkinson et al., 2011, 2013).

We selected sites with exposures of fluvial deposits located across mountain-front fans on the central interior bajada and along a feeder channel and proximal part of a fan on the eastern mountain front. This sampling strategy aimed to build as complete a record of aggradation as possible, considering the spatial variability in fan deposition. Sites comprised three from the eastern-draining Wadi Sahtan and the alluvial fan emanating from its apex at Rustaq on the Batinah Coastal plain (sites OM20/3–5; Fig. 3), and five sites from the interior fans of the central

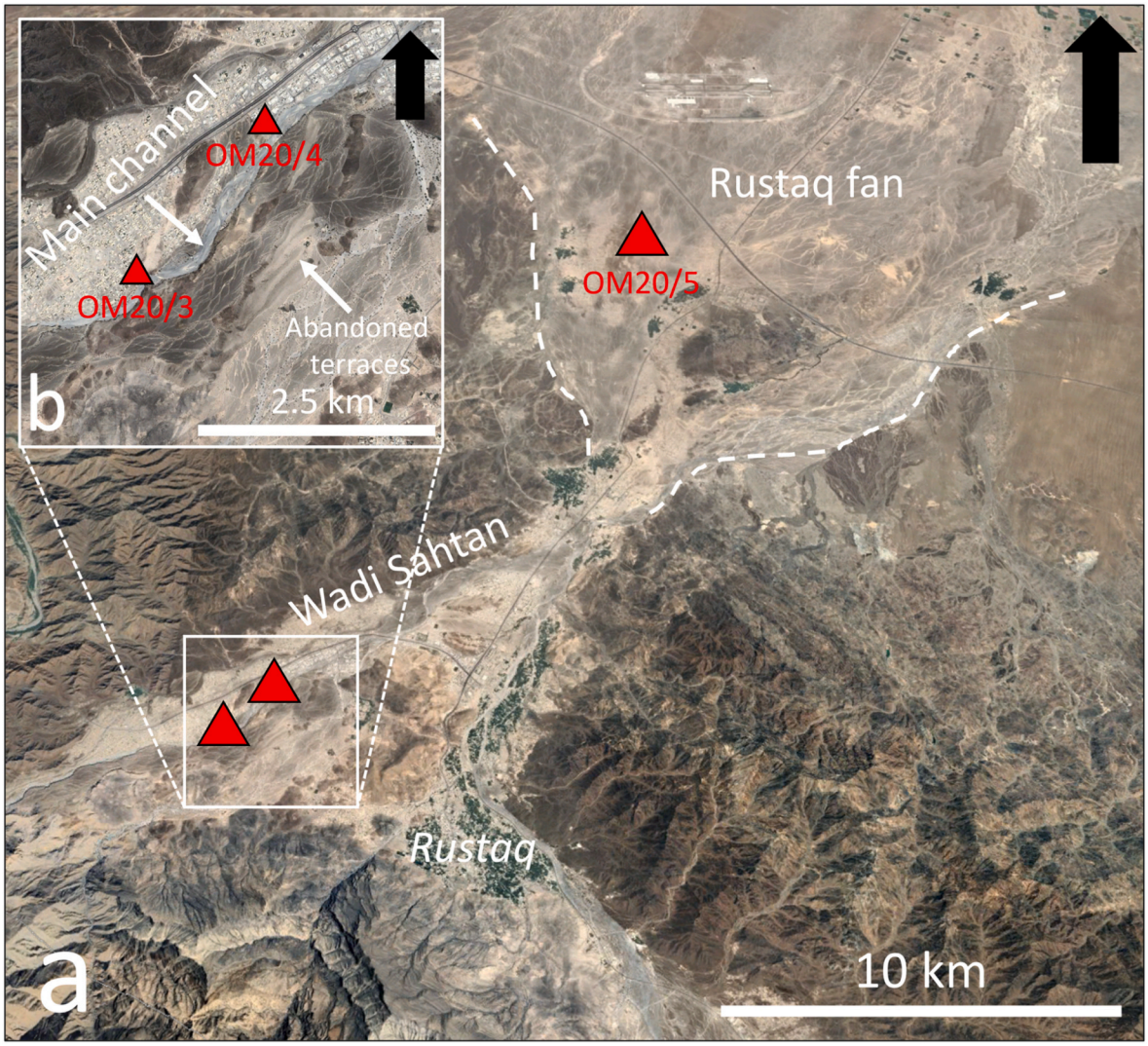

Fig. 3. **(a)** The location of sampled sites east of the Hajar drainage divide along Wadi Sahtan (OM20/3–4) and in the proximal part of the Rustaq fan (OM20/5). **(b)** The locations of sites OM20/3–4 in Wadi Sahtan, with valley-fill sequences exposed by the incised channel. Images from Google Earth Pro.

bajada (OM20/6–12; Fig. 4).

2.2. Wadi Sahtan and the rustaq fan

Wadi Sahtan drains north-east from a catchment in the central Hajar, forming an alluvial fan with an apex located near the town of Rustaq and extending down to the Arabian Sea coast (Fig. 3). The catchment is primarily composed of sedimentary geological units including sandstones and Jurassic carbonates that form the western portions of Jebel Ahkdar (Rousseau et al., 2005). The channel of Wadi Sahtan incises through valley-fill alluvium in the lower reaches of the catchment (Fig. 3b), exposing deep (~ 20 m) sections of fluvial sediments. These range in size from silty-sands to clast-supported conglomerates composed of large cobbles. Sites OM20/3 and OM20/4 are located along these exposed valley-fills, on the opposite side of the wadi to the Hayy al-Sarh Neolithic archaeological site which occupies an upper terrace (Bretzke et al., 2018). A fourth site, OM20/2 was also sampled just upstream from OM20/3 at the same sand unit as OM20/3/1 and −3/2. However, due to sampling within close proximity (<20 cm) to a conglomerate unit and the lack of field gamma spectrometry at this site, the sample is not presented (see Supplementary Information section 1.2.1). Downstream, Wadi Sahtan passes through a gap in the mountain front near Rustaq, resulting in the deposition of a large alluvial fan on the Batinah Coast. The fan is incised by smaller stream networks, exposing shallow (typically 1–5 m) sections of fluvial deposits such as site OM20/5 (Fig. 3).

2.3. The Ibri and Dhank fans

West of the Hajar drainage divide, large megafans emanate from apexes located at the towns of Ibri and Dhank on the interior mountain front (Fig. 4a). These fans are substantially more extensive than the Rustaq fan on the other side of the range and have formed in the foreland basin of the Hajar mountains that provides considerably more accommodation space than the much narrower Batinah Coastal zone (Rodgers and Gunatilaka, 2003). The fans are fed by large catchments draining mixed geologies composed of the Semail ophiolite, but also the limestones of the Hawasina nappes and the younger carbonates of the post-nappe units which outcrop at the mountain front (Glennie et al., 1973; Corradetti et al., 2020). Both fans backfill into their catchments, with the Ibri fan having two apexes, likely as the result of two merging fans. The Ibri and Dhank fans coalesce, forming a low-gradient plain stretching to the Rub'al Khali, with incised channels exposing sections of fluvial sands and gravels. Sites OM20/6 and OM20/12 are located close to the fan apexes at the mountain front (Fig. 4). OM20/6 is in close proximity to the Ibri mountain-front rock shelter site, which shows

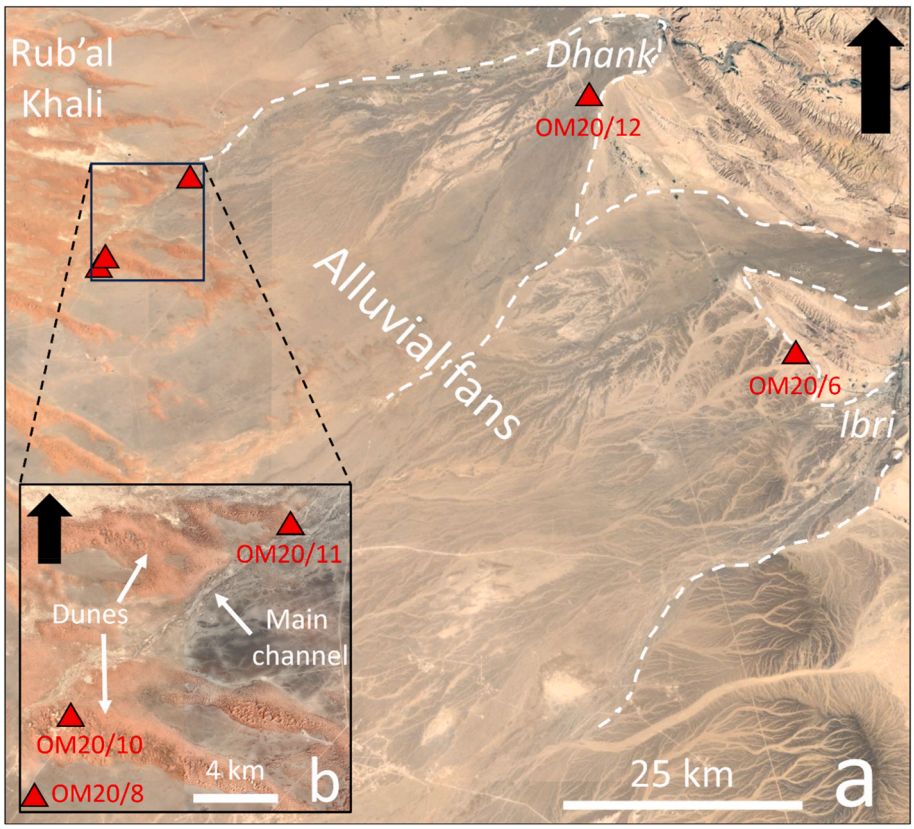

Fig. 4. **(a)** The location of sampled sites west of the Hajar drainage divide on the Ibri and Dhank fans. **(b)** Sites OM20/8, -/10 and -/11 in the medial-distal part of the Dhank fan where fan surfaces begin to become obscured by Rub'al Khali dunes. Images from Google Earth Pro.

evidence of Pleistocene human occupation (Parton and Bretzke, 2020). Sites OM20/8–11 are located in the medial-distal portion of the Dhank fan where fan surfaces begin to become obscured by aeolian sediments (Fig. 4b).

3. Methods

3.1. Luminescence dating

Luminescence dating samples were collected from units of fluvial sands from channel fill or overbank deposits using either opaque tubes hammered into sections or, where sediments were highly cemented, chiselled out as blocks. Samples were wrapped in light-tight plastic for transport to the laboratory. Samples were analysed at the Oxford Luminescence Dating Laboratory, University of Oxford. Under orange light conditions, light-exposed sediments were removed from the ends of tube samples and the outer surfaces of blocks. Sediments were then treated with 37% HCl and 30% H_2O_2 to remove carbonate and organic material, before undergoing sieving and density separation to isolate medium-coarse grained quartz. The quartz was then etched with 40% HF for 45 min and mounted on 9.8 mm aluminium discs as small aliquots of 2 mm diameter.

Ultra-violet quartz OSL signals were measured using Risø TL/OSL luminescence readers fitted with blue-light emitting diodes (470 nm) and calibrated $^{90}Sr/^{90}Y$ beta sources, using the single aliquot regenerative dose (SAR) protocol (Wintle and Murray, 2006; Murray and Wintle, 2003). OSL signals were measured at 125 °C for 40 s. A preheat temperature of 220 °C and a cutheat of 160 °C was used for all samples following pre-heat plateau and dose recovery tests (Fig. S1). D_es were calculated using the signal from the first 1 s of stimulation, and an averaged background taken from the final 20 s of stimulation was subtracted. The rejection criteria used to screen resulting D_e measurements included OSL IR depletion ratios (Duller, 2003), recycling and recuperation ratios (Murray and Wintle, 2003), a test signal (T_n) greater than 3 σ above background levels, and the fast ratio of Durcan and Duller (2011) (Table S1).

Inductively-coupled plasma mass spectrometry (ICP-MS) was used to measure ^{238}U, ^{232}Th and ^{40}K concentrations to calculate beta and gamma dose rates and, for samples where infinite matrix assumptions could not be made with respect to the gamma dose rate, in-situ gamma spectrometry was measured with an InSpector Canberra 1000 portable gamma spectrometer that was calibrated using the Oxford blocks prior to measurement (Rhodes and Schwenninger, 2007). The conversion factors of Guérin et al. (2017) were used to convert radionuclide concentrations into infinite matrix dose rates, and attenuation factors including etching depth (Bell, 1979), grain size range (Guérin et al., 2012) and an estimated water content of 5 ± 10% were accounted for. The central water content value is assumed based on previous luminescence analyses on alluvial sediments from the Hajar region and drylands more broadly (e.g. Blechschmidt et al., 2009; Parton et al., 2015a; Durcan et al., 2019; Mueller et al., 2022; Walsh et al., 2022a). The larger uncertainty value, relative to many previous studies in the region, used for water content aims to reflect the potentially wide-ranging moisture content likely experienced by alluvial sediments during the burial history. The conversion from dry to wet beta and gamma dose rates was based on attenuation factors accounting for the carbonate contents of samples following the approach outlined by Nathan and Mauz (2008), except for where gamma dose rates were measured in-situ (see supplementary information). Environmental dose rates were calculated using the Dose Rate and Age Calculator (DRAC, version 1.2; Durcan et al., 2015).

3.2. Sedimentology

Facies interpretations were undertaken in the field to determine streamflow conditions at the time of deposition, i.e. whether deposition was occurring under more sustained flow conditions or under similar, flashy flows relative to present. These interpretations were made using a simple facies model based on interpretations made for similar fluvial, or 'Scott-type', fans and braided stream facies in the region as well as other dryland contexts (e.g. Miall, 1977; Atkinson et al., 2013; Parton et al., 2015a; Bowman, 2019; Mueller et al., 2022; Walsh et al., 2022b). Fluvial fans are those on which deposition is primarily driven by braided-stream processes as opposed to more viscous debris flows (Harvey, 2011).

Sedimentary units indicative of more sustained streamflow, relative to present, are inferred to be where fans build thick conglomerate sequences of gravel-cobble sized clasts that are imbricated in the downstream direction (e.g. unit 2, Fig. 5c). Associated with these conglomerate units may be sand lenses that show evidence of low-angle bedding suggesting the formation of sand bars in stream systems (e.g. unit 4, Fig. 5b; Mueller et al., 2022). Laterally, these units often show the complex, multi-storey architecture of shallow (1–2 m) braided stream systems (e.g. unit 3, Fig. 5b). Interbedded with these conglomerate and sand deposits are finer silt-sand sediments with fine laminations and often evidence of bioturbation with root voids that are highly cemented by carbonate (e.g. units 1 and 3, Fig. 5a). These sediments are interpreted to be indicative of deposition onto stabilised floodplains during overbank flow and incipient palaeosol development (Parton et al., 2015a). By contrast, thin (<30 cm) units of sands and gravels with either horizontal or no bedding are interpreted as representing deposition under high velocity but short-lived floods (e.g. unit 1, Fig. 5c). Ephemeral flooding is typical of these systems today, often depositing similarly thin veneers of sand and gravel (e.g. Blechschmidt et al., 2009), with only the largest events reworking larger clasts.

To compliment field sedimentological interpretations, bulk sediment was also extracted from the luminescence dating samples for grain size analysis. Analysis was carried out using a laser granulometer (Malvern Mastersizer, 2000), with samples undergoing ultra-sonic displacement for 30 s before analysis commenced to ensure particle disaggregation. The characteristics of each grain size distribution were calculated from measurements made on three subsamples, enabling average particle size distributions to be determined. The GRADISTAT software (version 9.1) was used to calculate the percentages of sands (63 μm - 2 mm) and silts and clays (<63 μm) from these distributions, as well as modal grain size, sorting and skewness statistics (Blott and Pye, 2001).

3.3. Hierarchical cluster analysis of age and palaeoenvironmental data

Cluster analysis is a statistical approach for identifying groups within a dataset and has been previously applied to inventories of luminescence ages (e.g. Kalińska et al., 2022). It offers a more objective means of identifying periods of hydrological activity at regional scales than a qualitative assessment of many ages.

Luminescence and radiocarbon ages from this study and the literature were filtered to only include those from sedimentary contexts draining the Hajar interpreted by the original authors as representative of either more sustained streamflow conditions in fans and rivers or of lake highstands, relative to present (n = 93; Table S6). Any ages relating to deposits interpreted as being the result of ephemeral flooding events under relatively drier climate conditions where disregarded (e.g. examples in Rosenberg et al., 2012; Mueller et al., 2022; this study). These distances were computed as a measure of similarity between central age

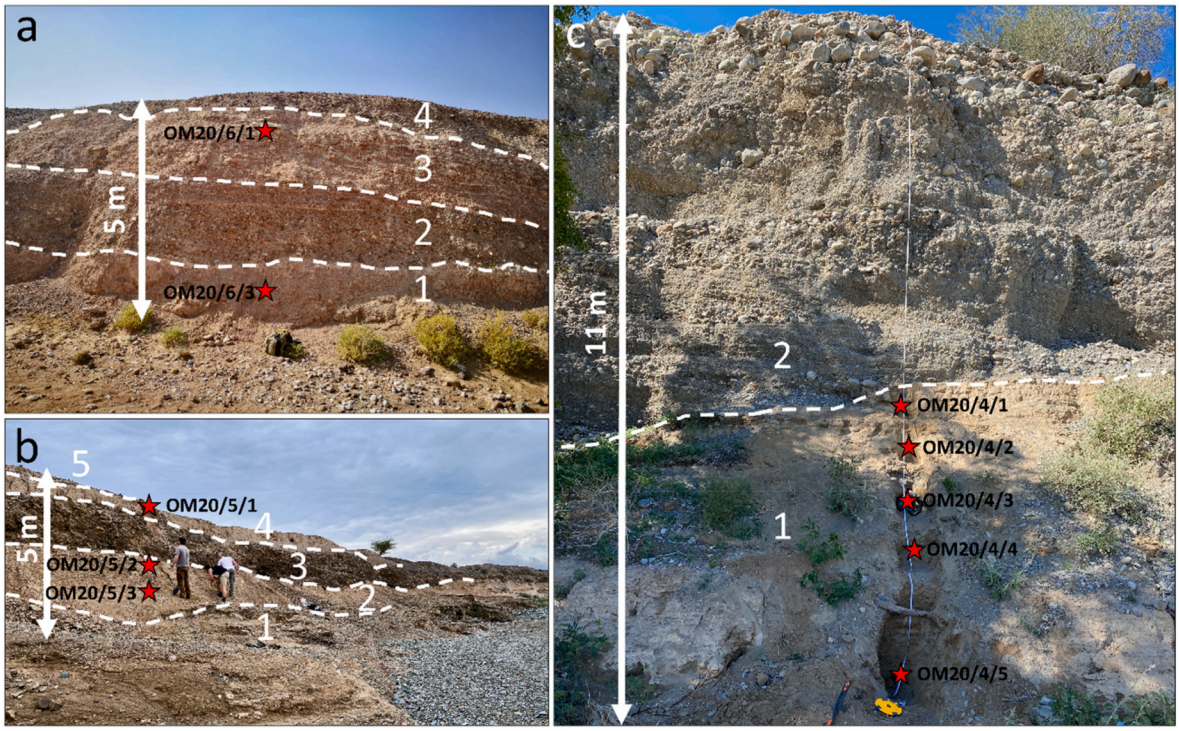

Fig. 5. Examples of the sections studied and their sedimentary interpretations. a) Site OM20/6: units 1 and 3 are overbank deposits of medium sands showing fine lamination and root voids. They are interstratified with conglomerate units which fine upwards from medium cobbles to gravels, representing cut and fill channel deposits (units 2 and 4). b) Site OM20/5 viewed laterally: Units 1, 3 and 5 are conglomerate deposits of cobbles and gravels. Unit 3 displays the lateral, multi-storey channel deposits typical of avulsing braided stream systems. Unit 2 is finely laminated silt-sand floodplain deposits with evidence of palaeosol development. Unit 4 is a unit of fluvial sand with weak bedding structures. c) Site OM20/4: Unit 1 is comprised of thin sheet-like deposits of interstratified fine sands and gravels with weak horizontal bedding, interpreted as rapid, short-lived flood events under ephemeral flow conditions, similar to present. Unit 2 is comprised of gravels to large cobbles that show some low angle bedding and are imbricated downstream, suggesting more sustained streamflow, relative to present. Red stars denote where samples for luminescence dating were taken.

values. Euclidean distance values were used to inform hierarchical clustering, whereby each member of the dataset is paired with its most similar neighbour, with groups then progressively paired with most similar groups until all values are incorporated. Resulting clusters of ages are then used to interpret when periods of more sustained flow occurred across the region, relative to present.

Table 1
Luminescence age results, including: the sampling depth, grain size, soil radionuclide concentrations (measured using ICP-MS), total environmental dose rate and its components, number of aliquots accepted out of total measured, relative overdispersion (OD), the age model applied for D_e calculation, final D_e and resulting age reported with 1σ errors. CAM: central age model (Galbraith et al., 1999), MAM: minimum age model (Galbraith and Laslett, 1993). Ages are reported to 1 decimal place, except for OM20/10/3 which is reported to 2 decimal places, with calculations made prior to rounding. For the two samples considered saturated, the minimum De and age are reported to the nearest integer.

Sample	Depth (m)	Grain size (μm)	K (%)	U (ppm)	Th (ppm)	Beta dose rate (Gy ka^{-1})	Gamma dose rate (Gy ka^{-1})	Cosmic dose rate (Gy ka^{-1})	Environmental dose rate (Gy ka^{-1})	n	OD (%)	Age model	D_e (Gy)	Age (ka)
OM20/3/1	10.30	90–150	1.22 ± 0.12	1.38 ± 0.14	5.44 ± 0.54	1.16 ± 0.16	0.73 ± 0.04	0.07 ± 0.01	1.96 ± 0.17	34/96	34	ADM	87.6 ± 5.9	44.8 ± 4.9
OM20/3/2	10.80	90–210	1.14 ± 0.11	1.31 ± 0.13	3.53 ± 0.35	1.04 ± 0.15	0.57 ± 0.07[a]	0.07 ± 0.01	1.67 ± 0.16	27/48	31	ADM	74.5 ± 5.0	44.5 ± 5.3
OM20/3/3	12.30	150–210	1.19 ± 0.12	1.12 ± 0.11	8.05 ± 0.81	1.13 ± 0.16	0.77 ± 0.1[a]	0.06 ± 0.01	1.95 ± 0.19	27/70	36	ADM	128.4 ± 8.5	65.8 ± 7.6
OM20/4/1	8.50	150–210	0.86 ± 0.09	1.48 ± 0.15	2.99 ± 0.3	0.83 ± 0.12	0.34 ± 0.02	0.08 ± 0.01	1.25 ± 0.12	8/48	27	ADM	>124	>100
OM20/4/2	8.75	150–210	0.93 ± 0.09	1.37 ± 0.14	3.65 ± 0.37	0.89 ± 0.13	0.53 ± 0.07[a]	0.07 ± 0.01	1.49 ± 0.08	17/48	24	ADM	93.2 ± 5.6	62.2 ± 7.0
OM20/4/4	9.60	90–250	0.87 ± 0.09	1.37 ± 0.14	3.04 ± 0.30	0.84 ± 0.12	0.49 ± 0.06[a]	0.07 ± 0.01	1.40 ± 0.13	55/95	23	ADM	109.0 ± 3.7	77.9 ± 7.9
OM20/4/5	10.40	150–210	0.70 ± 0.07	1.32 ± 0.13	2.63 ± 0.26	0.70 ± 0.1	0.71 ± 0.04	0.07 ± 0.01	1.47 ± 0.11	22/52	25	ADM	98.0 ± 5.6	66.6 ± 6.1
OM20/5/1	0.35	150–210	0.29 ± 0.03	0.45 ± 0.05	0.81 ± 0.08	0.27 ± 0.04	0.28 ± 0.02	0.22 ± 0.02	0.76 ± 0.05	43/113	66	ADM	50.6 ± 4.4	66.2 ± 7.1
OM20/5/2	2.60	150–210	0.40 ± 0.04	0.73 ± 0.07	1.60 ± 0.16	0.40 ± 0.06	0.33 ± 0.02	0.15 ± 0.02	0.88 ± 0.06	23/48	22	ADM	>97	>110
OM20/5/3	4.50	150–210	0.19 ± 0.02	0.65 ± 0.07	0.62 ± 0.06	0.22 ± 0.03	0.3 ± 0.02	0.12 ± 0.01	0.64 ± 0.04	15/40	68	ADM	67.5 ± 11.2	105.4 ± 18.6
OM20/6/1	1.50	180–210	0.27 ± 0.03	0.41 ± 0.04	1.13 ± 0.11	0.26 ± 0.04	0.19 ± 0.01	0.17 ± 0.01	0.61 ± 0.04	16/32	26	ADM	185.4 ± 12.6	302.6 ± 29.3
OM20/6/3	4.80	125–180	0.36 ± 0.04	0.50 ± 0.05	1.23 ± 0.12	0.34 ± 0.05	0.21 ± 0.01	0.12 ± 0.01	0.67 ± 0.05	19/34	21	ADM	248.1 ± 13.2	372.5 ± 35.6
OM20/8/1	0.50	150–210	0.37 ± 0.04	1.05 ± 0.11	0.06 ± 0.01	0.38 ± 0.06	0.47 ± 0.03	0.2 ± 0.02	1.05 ± 0.07	33/48	22	ADM	93.4 ± 4.0	88.9 ± 6.7
OM20/8/2	0.90	150–250	0.16 ± 0.02	0.46 ± 0.05	0.03 ± 0.00	0.16 ± 0.03	0.28 ± 0.02	0.18 ± 0.02	0.63 ± 0.04	27/48	29	ADM	82.5 ± 4.8	131.8 ± 10.7
OM20/10/3	1.80	150–180	0.81 ± 0.08	0.83 ± 0.08	1.30 ± 0.13	0.70 ± 0.1	0.34 ± 0.04[a]	0.18 ± 0.02	1.22 ± 0.11	13/48	83	MAM	0.20 ± 0.04	0.16 ± 0.0.04
OM20/11/1	0.30	150–180	1.21 ± 0.12	0.45 ± 0.05	0.91 ± 0.09	0.93 ± 0.14	0.38 ± 0.05[a]	0.22 ± 0.02	1.53 ± 0.15	28/48	25	MAM	3.7 ± 0.2	2.4 ± 0.3
OM20/11/2	0.75	150–180	0.62 ± 0.06	0.78 ± 0.08	1.20 ± 0.12	0.55 ± 0.08	0.28 ± 0.04[a]	0.19 ± 0.02	1.03 ± 0.09	36/48	63	MAM	3.5 ± 0.3	3.4 ± 0.4
OM20/11/3	1.40	150–180	0.34 ± 0.03	0.51 ± 0.05	0.38 ± 0.04	0.31 ± 0.04	0.15 ± 0.02[a]	0.17 ± 0.02	0.63 ± 0.05	41/48	56	MAM	4.2 ± 0.3	6.6 ± 0.7
OM20/12/1	0.30	150–180	0.34 ± 0.03	1.07 ± 0.11	0.70 ± 0.07	0.38 ± 0.05	0.31 ± 0.02	0.23 ± 0.02	0.92 ± 0.06	44/48	42	ADM	23.3 ± 1.6	25.5 ± 2.5
OM20/12/2	2.60	90–150	0.16 ± 0.02	0.38 ± 0.04	0.15 ± 0.02	0.16 ± 0.03	0.4 ± 0.02	0.15 ± 0.02	0.71 ± 0.04	25/32	33	ADM	110.7 ± 8.8	156.3 ± 14.9

[a] The gamma dose rates of these samples were calculated based on ICP-MS measurements of radionuclides and not in-situ gamma spectrometry.

4. Results

4.1. Chronology

In total, twenty samples were dated using quartz OSL signals (Table 1; Table S3). In general, luminescence signals that passed other rejection criteria tended to be dominated by the fast component, yielding fast ratios >20 (Durcan and Duller, 2011; Table S1). An example natural signal for an aliquot of sample OM20/3/3 is shown in Fig. 6a. The proportion of aliquots of samples from Wadi Sahtan and the Rustaq fan that failed rejection criteria were higher than western samples (Table 1; Table S1). These samples suffered from pervasive contamination from IR sensitive minerals, leading to higher aliquot rejection rates than samples from the Ibri and Dhank fans (see supplementary materials for more detail). Contaminants were pervasive despite repeating heavy liquid separations and treating some samples with fluorosilicic acid for 2 weeks (e.g. Woor et al., 2022b). Therefore, high numbers of aliquots were measured for samples from Wadi Sahtan and the Rustaq fan to maximise pure quartz signals.

Two samples had >25% of D_es either in or close to saturation (samples OM20/4/1 and OM20/5/2). Therefore, they are ascribed a minimum age based on the average dose model (ADM) D_e for aliquots with L_n/T_n ratios intercepting the dose response curve, due to the potential truncation of the dose distribution (Table 1; see the supplementary material for more discussion of signal saturation). OM20/4/1 (>100 ka) is significantly older than the underlying OM20/4/2 (62.2 ± 7.0), which may be due to OM20/4/1 having a very low sample size at just 8 aliquots passing rejection criteria (Table 1). This could mean that the dose distribution is very poorly characterised. Therefore, we are not confident in this age and it is excluded from the discussion.

For most samples, D_e distributions were normally distributed around a central value, although they show broad scatters and overdispersions which range between 21 and 68%, as well as an overdispersion of 83% for the low D_e sample OM20/10/3 (Table 1). This wide range of overdispersion values for gaussian dose distributions is typical of Hajar alluvial sediments (e.g. Parton et al., 2015a; Hoffmann et al., 2015). Previous studies (e.g. Blechschmidt et al., 2009; Parton et al., 2015a) have speculated that the very broad, gaussian-like D_e scatters observed in Hajar alluvial sediments may be the result of beta heterogeneity. Heterogeneity in beta dose rate is more likely to be present where

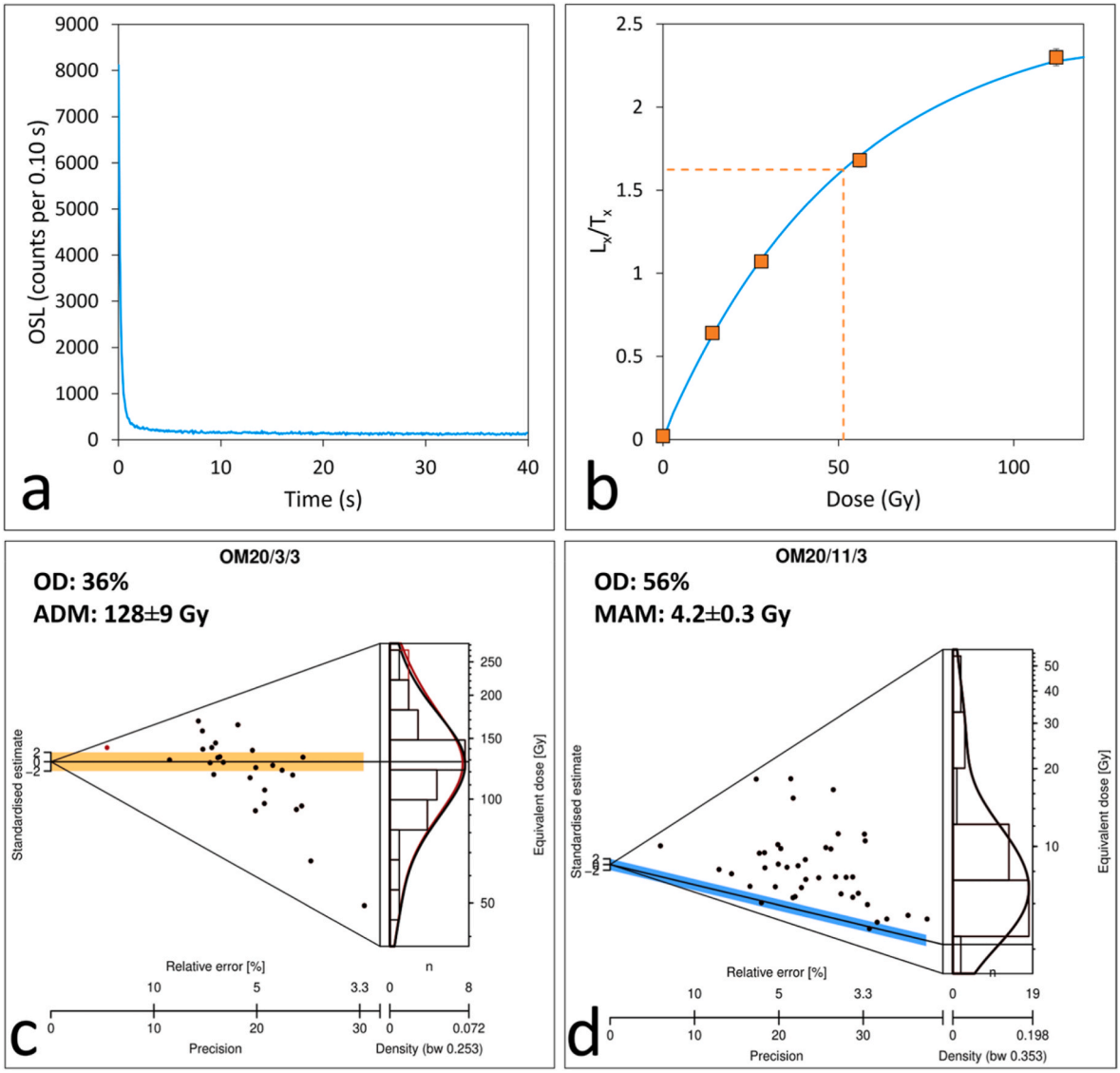

Fig. 6. (a) An example OSL signal for an aliquot of sample OM20/3/3, and the dose response curve measured for the same signal **(b).** Below are abanico plots showing example D_e distributions for **(c)** the broadly gaussian sample OM20/3/3 and **(d)** the positively skewed sample OM20/11/3. The ADM and MAM D_es are displayed with the orange and blue bars, respectively, as well as relative overdispersion (OD).

sediments have low radionuclide concentrations, are subject to post-depositional carbonate growth, have coarse grain sizes and low K-feldspar contents (Nathan et al., 2003; Mayya et al., 2006; Guérin et al., 2015), as is the case with alluvial material from the Hajar (e.g. Blechschmidt et al., 2009; Parton et al., 2015a; Hoffmann et al., 2015; Woor et al., 2022b). For samples from the Ibri and Dhank fans in particular, radionuclide concentrations are especially low compared to those from the Wadi Sahtan and Rustaq fan, with typical values of K <1 % and U and Th < 1 ppm (Table 1); samples from Wadi Sahtan and the Rustaq fan have previously been shown to have low K-feldspar contents (Woor et al., 2022b), and the samples in this study are comprised of up to 35% carbonate by weight (Table S5).

Partial bleaching is also often an issue in alluvial fan sediments, contributing to the scatter in D_e distributions (Rittenour, 2008). However, the broad, gaussian-like D_e distributions in our samples are not typical of the skewed distributions expected from sediments with significant partial bleaching (e.g. Rodnight et al., 2006). Fan and river sediments from dryland contexts often show broad D_e distributions, with authors using central age approaches for D_e calculation rather than minimum age approaches (e.g. Kenworthy et al., 2014; Durcan et al., 2019). Moreover, it is likely that the residual dose effect of partial bleaching would become less important with sample age, due to the larger uncertainties associated with D_e values (e.g. Jain et al., 2004). Blechschmidt et al. (2009) tested signal resetting from sediments transported during a modern flash flood on a fan in the southern Hajar to test the extent of bleaching in the modern day system. They record only a small residual dose (<1 ka) from these sediments, and assuming similar deposition conditions for the samples in this study, this suggests that the effects of partial bleaching would not be notable relative to the Pleistocene-age sediments dated.

Based on these considerations, and the use of central ages in previous studies dating Hajar alluvium with similar, broadly scattered D_e distributions (e.g. Parton et al., 2015a; Mueller et al., 2022; Beuzen-Waller et al., 2022), the ADM is used to calculate all final D_es for Pleistocene sediments (Table 1). The ADM is based on the arithmetic mean of D_es, rather than the weighted mean of the central age model (CAM), which is more appropriate for samples where beta heterogeneity may be suspected and does not bias ages towards younger values with lower uncertainties, as may be the case with CAM (Guérin et al., 2017). This is important in this context where D_es are often in the upper portion of the dose response curve, beyond the characteristic dose (D_0), as is the case for many of the Pleistocene samples in this study. D_es calculated using the ADM, CAM and minimum age model (MAM) are shown in Table S3 for comparison.

In contrast, the Holocene samples have skewed D_e distributions with many smaller values and long 'tails' of larger values, suggestive of partial bleaching (e.g. Fig. 6d). Similar distributions have been previously reported from Hajar alluvial sediments (e.g. Hoffmann et al., 2015; Mueller et al., 2022), although are less common than the gaussian-like distributions described above. Partial bleaching is potentially more of an issue in these younger sediments because the residual dose will constitute a greater component of the total De measured, and, therefore, will result in greater inaccuracy in the age (relative to older samples) if the effects of partial bleaching within a dose distribution are not taken into account. For these samples, the decision tree method of Arnold et al. (2007), developed using multi-grain aliquot D_e distributions for North American arroyo sediments, with comparable shallow channel deposition contexts, was used to establish the appropriate age model to employ. This approach suggests that the Holocene fan sediments dated in this study includes signals that were not fully reset prior to burial, as they all have skewness and kurtosis values >1σ or have relative overdispersions and standard deviations relative to the weighted mean D_e >40% (Table S4). Therefore, final D_es for the Holocene samples were calculated using the minimum age model (MAM) with a σ_b value of 0.055, calculated from the mean overdispersion of D_es from dose recovery tests (Galbraith et al., 1999; Galbraith and Roberts, 2012). Using the 'Luminescence' R package, we estimate that there are ~ 95 grains per 2 mm aliquot for the MAM samples as they all have grain size ranges of 150–180 μm and assuming a packing density of 0.65 (Kreutzer et al., 2012).

Ages show good chrono-stratigraphic agreement with a considerable range across the sites sampled, spanning the historical period (OM20/10/3) to 372.5 ± 35.6 ka (OM20/6/3; Table 1). Relative age uncertainties range from 8 % (OM20/8/1) to 18% (OM20/5/3), with the very young age of OM20/10/3 giving an outlying relative uncertainty of 21%. Ages from Wadi Sahtan and the Rustaq fan fall primarily between 70 and 40 ka, although the lower unit of site OM20/5 was older at 105.4 ± 18.6 ka (Table 1). For the Ibri and Dhank fans, resulting ages are more spread across sites at ~ 370-300 ka, 160 ka, 130 ka, 90 ka and 7–0 ka (Table 1).

4.2. Sedimentary descriptions and chronostratigraphic relationships

The dated samples have modal grain sizes ranging from very fine sand (63–125 μm) to coarse sand (0.5–1 mm) (Table 2). Some samples comprise up to 50% silt and clay (e.g. OM20/6/3, OM20/12/1); others exceeded 90% sand (e.g. OM20/11/1, OM20/11/3) (Table 2). All samples except OM20/10/3 and OM20/11/1, which are moderately sorted, display poor or very poor sorting and distributions are typically either symmetrical or very fine-skewed. Of course, these samples represent facies where tube or block samples could be taken for OSL dating and so do not capture coarse gravel (2–60 mm diameter) or cobble (>60 mm diameter) fractions, but they provide extra information about the types of sediment deposited during the periods identified from OSL ages.

The eight exposures both west and east of the Hajar watershed divide were composed of fluvial deposits ranging from silty-sand units to matrix supported conglomerates (Figs. 5, 7 and 8). The stratigraphic interpretations and associations for each section are as follows:

OM20/3: The base of the section intersects with the modern channel floor where there is an exposure of ~ 1 m of conglomerate material (Fig. 7). Above is a sharp contact with 5.75 m of very fine palustrine silt-sands dated to 65.8 ± 7.6 ka (sample OM20/3/3; Tables 1 and 2) which display fine lamination and are highly cemented, becoming less friable with depth, yet lack evidence of palaeosol development so could indicate deposition in a low-energy, ponded environment (Miall, 1977). These sediments are overlain by a coarser unit of low-angle (<15°), planar-bedded fluvial sands which fine upwards dated to 44.5 ± 5.3 and 44.8 ± 4.9 ka (OM20/3/2, -/1). Above is a sharp contact with channel infills of gravel and coarse sands and larger, poorly sorted semi-rounded gravels and cobbles comprising the upper clast-supported conglomerate unit. The basal 1.5 m of this unit displays weak planar cross bedding indicative of low-velocity streamflow (Bowman, 2019).

OM20/4: The basal unit above the modern channel is comprised of 0.8 m of poorly sorted, very fine fluvial sand dated to 66.6 ± 6.1 ka (OM20/4/5) (Fig. 7) with occasional gravel inclusions. These sands coarsen upwards into a thin layer (<0.1 m) of sands and fine gravels. This is overlain by a thin unit (0.2 m) of very fine fluvial sand dated to 77.9 ± 7.9 ka (OM20/4/4). This represents an age reversal with the under- and overlying ages, but is still within 1σ errors of OM20/4/5 so is attributed to the same period. Above is a series of thin gravel lenses interrupting the deposition of very fine sands and coarse silts with gravel inclusions that are 1.5 m thick, with sample OM20/4/2 taken from the penultimate sand unit dated to 62.2 ± 7.0 ka (Table 2). The sharp contacts between these gravel lenses and over- and underlying sands as well as their horizontal bedding suggest they are the result of sheetfloods under a flashy flow regime (Miall, 1977). Overlying this are a series of bedded channel lag deposits comprising gravels and small pebbles and semi-to angular gravels and well-rounded pebbles and cobbles displaying imbrication downstream. Above is a clast-supported conglomerate of larger pebbles and cobbles with no apparent bedding, comprising the upper 4 m of the section.

Table 2
Grain size data from the <2 mm fractions of the samples taken for luminescence dating, calculated using the GRADISTAT software (version 9.1; Blott and Pye, 2001).

Sample	Silts and clays (%)	Sands (%)	Modal grain size (μm)	Description	Sorting (σ)	Description	Skewness (*Sk*)	Description
OM20/3/1	44.3	55.7	84.5	Very fine sand	2.9	Poorly sorted	−0.2	Fine-skewed
OM20/3/2	31.7	68.3	106.4	Very fine sand	2.4	Poorly sorted	−0.1	Fine-skewed
OM20/3/3	38.0	62.0	119.3	Very fine sand	4.4	Very poorly sorted	−0.2	Fine-skewed
OM20/4/2	27.3	72.7	94.8	Very fine sand	2.5	Poorly sorted	0.0	Symmetrical
OM20/4/4	47.1	52.9	84.5	Very fine sand	3.1	Poorly sorted	−0.1	Fine-skewed
OM20/4/5	27.4	72.6	94.8	Very fine sand	2.7	Poorly sorted	0.0	Symmetrical
OM20/5/1	23.6	76.4	238.1	Fine sand	3.6	Poorly sorted	−0.5	Very fine-skewed
OM20/5/2	34.8	65.2	94.8	Very fine sand	6.6	Very poorly sorted	−0.1	Fine-skewed
OM20/5/3	23.1	76.9	150.2	Fine sand	4.1	Very poorly sorted	−0.1	Fine-skewed
OM20/6/1	44.3	55.7	475.1	Medium sand	5.1	Very poorly sorted	0.0	Symmetrical
OM20/6/3	50.0	50.0	212.2	Medium sand	5.2	Very poorly sorted	0.0	Symmetrical
OM20/8/1	35.0	65.0	475.1	Medium sand	5.3	Very poorly sorted	−0.4	Very fine-skewed
OM20/8/2	22.6	77.4	752.9	Coarse sand	4.0	Very poorly sorted	−0.3	Very fine-skewed
OM20/10/3	12.7	87.3	119.3	Very fine sand	1.8	Moderately sorted	−0.3	Very fine-skewed
OM20/11/1	5.9	94.1	189.1	Fine sand	2.0	Moderately sorted	0.1	Symmetrical
OM20/11/2	26.5	73.5	133.9	Fine sand	2.5	Poorly sorted	−0.3	Fine-skewed
OM20/11/3	3.7	96.3	189.1	Fine sand	2.1	Poorly sorted	0.2	Coarse-skewed
OM20/12/1	50.3	49.7	119.3	Very fine sand	7.2	Very poorly sorted	0.1	Symmetrical
OM20/12/2	48.8	51.2	106.4	Very fine sand	4.7	Very poorly sorted	0.0	Symmetrical

OM20/5: This section extends to a height of 5.75 m above the modern channel. The basal unit is comprised of highly indurated pebbles within a calcareous matrix of silt-sands. This is overlain by a unit of weakly laminated fine sands that is 2 m thick (Table 2; Fig. 7), the base of which yielded an age of 105.4 ± 18.6 ka (OM20/5/3). This unit is highly cemented by carbonates and preserves pinprick root voids, indicative of deposition overbank of the main channel and of incipient palaeosol development (Parton et al., 2015a). Above is a sharp contact with a channel infill of gravels and small, imbricated pebbles in a sandy matrix with planar bedding typical of shallow, avulsing alluvial channels (Miall, 1977). This overlain by a conglomerate of larger pebbles and cobbles in a gravelly matrix. Viewing the exposure laterally, multiple channel scour and fill sequences are apparent in this unit, reaffirming the interpretation of a dynamic system of braided channels on the fan surface (Figs. 5 and 7). Deposition is interrupted at 0.5 m by a lens of weakly bedded fine fluvial sands which was dated to 66.2 ± 7.1 ka (OM20/5/1; Table 2). The top of the sequence is a thin (0.1 m) unit of pebbles and cobbles forming a desert pavement of varnished clasts on the relict fan surface above the sequence.

OM20/6: The base of this section consists of 1 m of highly calcareous, weakly laminated and well-cemented sands deposited in an overbank setting dated to 372.5 ± 35.6 ka (OM20/6/3; Fig. 8). The presence of root voids and dark staining suggests palaeosol development (Parton et al., 2015a). Above this is a sharp contact with a conglomerate unit of gravels and semi-rounded pebbles and cobbles (1.5 m thick). Channel fill sequences are evident, fining upwards into planar bedded gravels and sands which indicate channel avulsion across the fan surface (Bowman, 2019). Again, this conglomerate unit is overlain by a sharp contact with a palaeosol unit comprised of sands with weak lamination suggesting its gradual accumulation in an overbank setting dated to 302.6 ± 29.3 ka (OM20/6/1; Table 2). The section is topped with another conglomerate unit of channel lag deposits which forms the overlying desert pavement.

OM20/8: The basal 0.3 m consists of highly cemented, coarse sand dated to 131.8 ± 10.7 ka (OM20/8/2) (Fig. 8) with occasional small clasts indicative of low, overbank flow regimes (Harvey, 2011). Deposition is interrupted by a sheet of gravels (0.1 m thick), before recommencing as a unit of sands with angular gravel inclusions and no discernible bedding architecture dated to 88.9 ± 6.7 ka (OM20/8/1). In the distal areas of large fans, unconfined sheetflooding in low-energy, ponded environments is more likely (Moscariello, 2018), so we interpret these units to represent gradual accumulation with occasional larger floods evidenced by gravel sheets.

OM20/10: The base of this sequence is the upper 0.5 m of the underlying playa sediments composed of very fine, laminated sands dated to 0.16 ± 0.04 ka (OM20/10/3; Fig. 8). These playa sands are interpreted as being derived from runoff from surrounding dunes and direct aeolian input into the basin because they show moderate sorting in comparison to typically poorly sorted sediments of fluvial origin (Table 2). This is overlain by 1.5 m of modern aeolian dune sands from the flanks of a large star dune.

OM20/11: The basal 0.8 m of this section is comprised of fluvial sands and gravels that fine upwards into coarse sands dated to 6.6 ± 0.7 ka (OM20/11/3; Fig. 8). Above, there is a sharp contact with 0.4 m of bedded channel lags of gravel and coarse sands, interspersed with occasional lenses of coarse, semi-rounded gravels. This unit terminates with another sharp contact into a bed of very fine fluvial sands dated to 3.4 ± 0.4 ka (OM20/11/2) topped with a thin lens (<0.1 m) of gravels. The uppermost fluvial unit of fine sand is moderately sorted, whereas the underlying units are poorly sorted and dates to 2.4 ± 0.3 ka (OM20/11/1; Table 2). This could indicate the reworking of aeolian material on fan surfaces by flashy flows. The section is overlain by a veneer of modern aeolian sands <0.1 m thick.

OM20/12: The base consists of 1.45 m of gravels and pebbles cemented within a calcareous matrix of silt-sands (Fig. 8). Above is a thin (0.25 m) unit of very fine, weakly-bedded and highly cemented fluvial sand with occasional inclusions of small clasts deposited in an overbank context dated to 156.3 ± 14.9 ka (OM20/12/2). Overlying are poorly sorted fluvial sands and gravels and a conglomerate unit of imbricated pebbles (1.3 m). A second unit of silt-sands with small gravel inclusions indicating proximal floodplain deposition 1.2 m thick then fines upwards and is dated to 25.5 ± 2.5 ka (OM20/12/1). The section is capped by 0.1 m of conglomerate material forming an overlying desert pavement.

4.3. Hierarchical clustering

A dendrogram was used to visualise the hierarchical cluster analysis of the new ages from this study and the fluvial and lake ages included from the literature (Fig. 9a). The average silhouette approach offers a means of determining the most appropriate number of clusters (k value) at which to cut the dendrogram, whereby the k value with the highest average silhouette score defines the point at which groups are the most different to each other whilst being the most internally similar (Rousseeuw, 1987). The silhouette score of k = 10 is the highest, meaning that 10 groups is the optimum for this dataset (Fig. 9b).

For each group, simple descriptive statistics were calculated (Table 3). The mean ages and interquartile ranges for each group are used to infer periods of fan aggradation under more sustained streamflow conditions, relative to present. For the majority of groups, standard

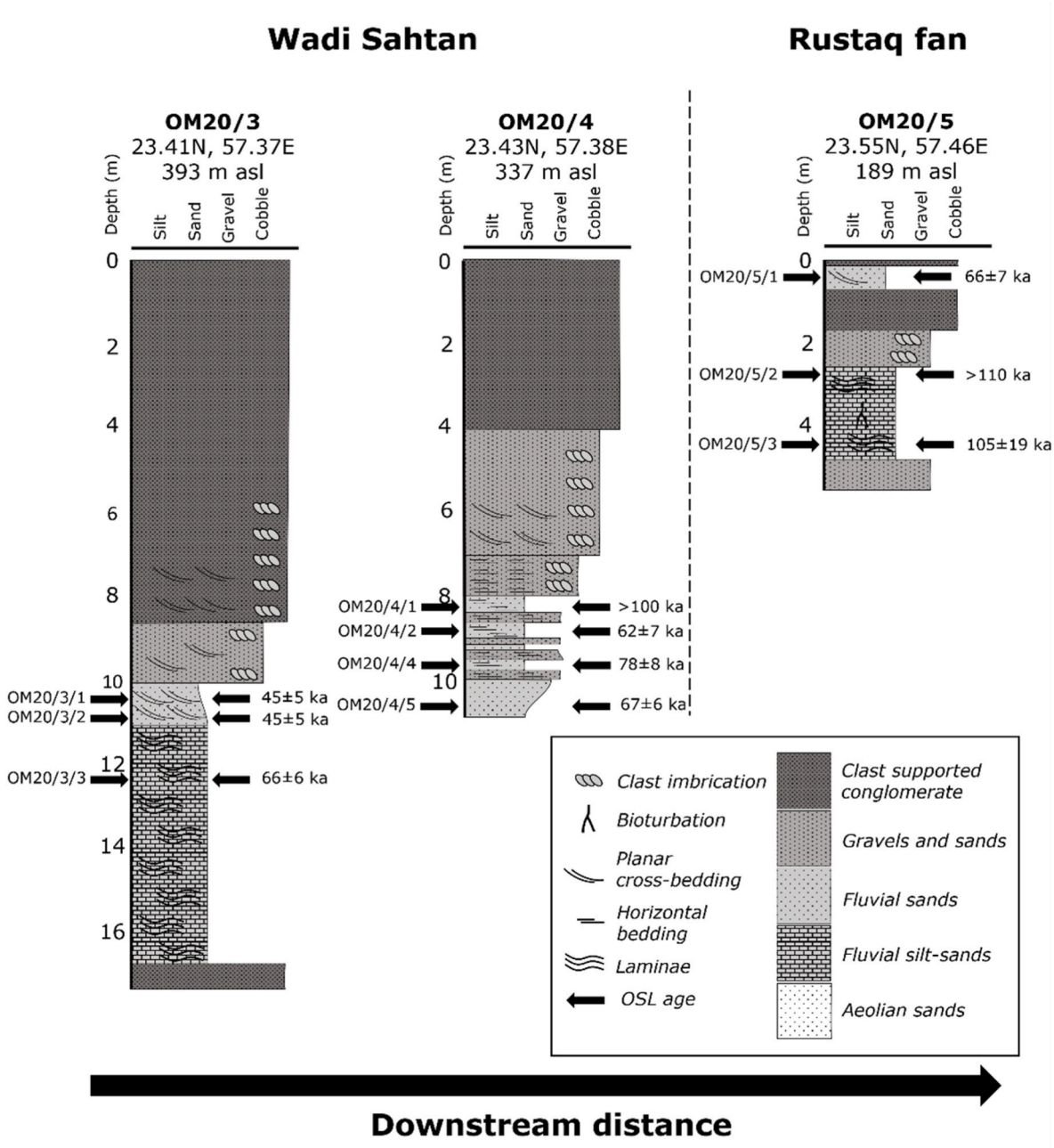

Fig. 7. Stratigraphic logs of sites from the eastern Hajar (OM20/3–5). Sampling locations, field sedimentological observations and OSL dating results are shown.

deviations lie within one precessional cycle (~ 23 ka) around the mean age; groups 7 and 10 are exceptions. Group interquartile ranges generally increase in line with mean age. Groups 7, 9 and 10 only returned very small numbers of ages (n = 1, 3 and 2, respectively). For groups 7 and 10, only the mean age is used to suggest a period of fan aggradation, acknowledging that low sample sizes may be an artifact of noise and sampling.

5. Discussion

5.1. Palaeoenvironmental interpretation

Together, the chronologies and sedimentary interpretations of the alluvial records in the central Hajar represent periods of aggradation back to 400 ka (Fig. 10; Table 4). Site OM20/6 is comprised of silty palaeosol units with laminae indicating gradual accumulation, likely as the result of seasonal flooding onto a stabilised floodplain, dated to ~ 370-300 ka (Table 2; Table 3). These periods of floodplain accumulation are punctuated by the aggradation of fluvial conglomerates and sands and gravel, indicating an environment characterised by channel avulsion and the development of braided streams and point bars on fan surfaces. Aggradation phases from the southern megafans of the interior bajada have been previously dated within errors of the ages presented from OM20/6 (Blechschmidt et al., 2009), although large dating errors mean that attributing them discretely to increased IOSM rainfall with a 23 ka periodicity is impossible. However, these ages correspond with terminal Northern Hemisphere interglacial conditions during MIS 11/9 and higher IOSM rainfall recorded in the Hoti Cave speleothem (Fleitmann et al., 2003; Lisiecki and Raymo, 2005).

The lower unit of OM20/12 records fan aggradation at 156.3 ± 14.9 ka. The conglomerate unit surrounding the sandy layer of OM20/12 shows increased channel activity which may be attributable to this

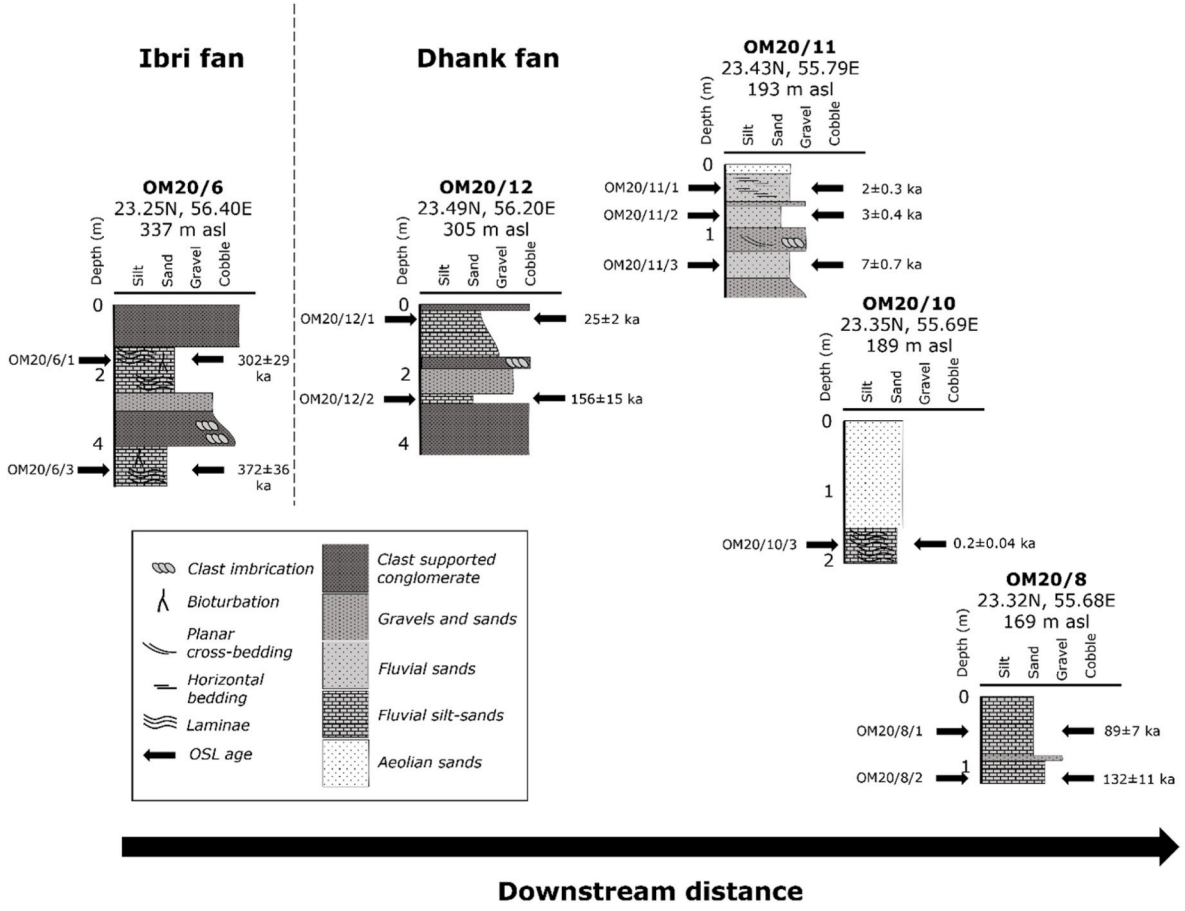

Fig. 8. Stratigraphic logs of sites from the western Hajar (OM20/6–12). Sampling locations, field sedimentological observations and OSL dating results are shown. Note the change of scale for sites OM20/11, -/10 and -/8.

period (Fig. 8). Again, this coincides with increased precipitation interpreted from biological and geochemical proxies from marine sediments and dated to ~ 150-160 ka during MIS 6 (e.g. Clemens and Prell, 2003). Whilst there is no growth in the Hoti Cave speleothem at this time (Fleitmann and Matter, 2009), numerous alluvial fan records show increased drainage activity (e.g. Parton et al., 2015a; Moraetis et al., 2020; Mueller et al., 2022), with an age cluster centred on 143.8 ka (Fig. 10).

The next phase of aggradation across the sites is recorded at 131.8 ± 10.7 ka in the basal unit of OM20/8, comprised of coarse, overbank sands and small gravels. This coincides with precessional maxima at ~ 130 ka at the transition from MIS 6 to 5e (Fig. 10). MIS 5e ages are reported from other alluvial sediments across south-east Arabia, with aggradation of the distal part of the Dhank fan occurring synchronously with that of alluvial fan aggradation at Remah to the north (Farrant et al., 2012) and alluvial sediment deposition underlying more recent aeolian deposits in the Wahiba Sands to the south (Preusser et al., 2002). Palaeolake Saiwan, also located at the distal extremity of the southern megafans, similarly records intensified hydrological conditions from 132–104 ka (Rosenberg et al., 2012). Increased monsoon rainfall is evidenced by palaeo-productivity proxies such as bromine concentrations from the Arabian Sea (Ziegler et al., 2010; Caley et al., 2011), as well as the Hoti Cave speleothem record in the central Hajar which shows very low $\delta^{18}O$ values at this time (Fleitmann and Matter, 2009). The coarse sediments of OM20/8/2 indicate that flow was regularly occurring from mountain catchments to the medial-distal extremities of the interior fans (Table 2). The low gradient of the fan and the finer grain sizes, relative to more proximal locations, suggests that these down-fan reaches would have been characterised by low-energy seasonal flows (Table 4). This is consistent with an environment comprised of shallow wetlands and low-gradient plains typical for large fluvial fans (e.g. Moscariello, 2018).

Site OM20/5 on the Rustaq fan shows aggradation in a stabilised overbank setting at 105.4 ± 18.6 ka, with evidence of incipient palaeosol formation based on the presence of root voids (Table 4). Fan aggradation has not been commonly reported during MIS 5c, with the only other site located in the UAE dating to 110 ± 6 (Atkinson et al., 2013). However, lake highstands in the Saiwan basin at the termini of the southern Hajar megafans coincide with this age, indicating more widespread hydrological activity (Rosenberg et al., 2012), resulting in a cluster of ages centred on 111.6 ka (Fig. 10).

The upper unit at site OM20/8 shows the aggradation of the distal end of the Dhank fan at 88.9 ± 6.7 ka (Fig. 8). Similarly, fan activation is recorded further north in the UAE during early MIS 5a (90–76 ka) where the deposition of silts and gravels has been observed closer to the mountain front (Atkinson et al., 2013) (Fig. 10). The upper deposit of OM20/8 suggests that the site was characterised by intermittent drainage connections with feeder catchments that were perhaps similar to or slightly more sustained than today. Evidence for speleothem growth during MIS 5a at Hoti Cave is absent until 82 ka (Fleitmann et al., 2003). Therefore, the earlier ages recorded at this site and from previously dated fan deposits in the UAE may be evidence of increasing fluvial activity in early MIS 5a, preceding a sufficient groundwater/throughflow threshold for speleothem growth. Indeed, an age cluster centred at 87.1 ka suggests an earlier increase in hydrological conditions with the onset of the precessional peak (Fig. 10).

The next recorded phase of aggradation is during late MIS 4–3, with ages from Wadi Sahtan and the Rustaq fan between ~ 67-45 ka (Fig. 7).

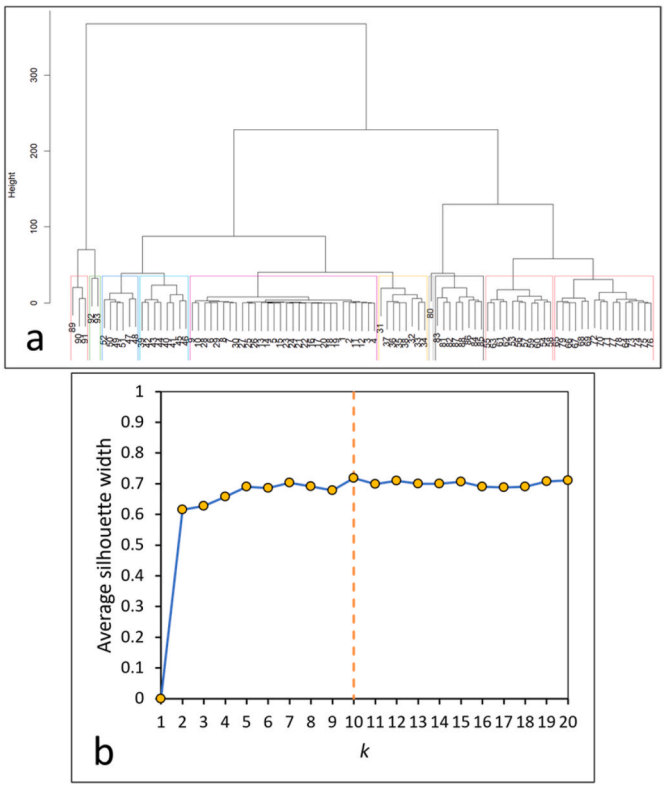

Fig. 9. **(a)** Dendrogram of clustered ages. Each age is represented by a number (1–93) and paired with its nearest neighbour at the bottom of the plot. Coloured boxes show the groups defined based on similarity (k = 10). See Table S6 for referenced ages included in this analysis. **(b)** Average silhouette widths for different k values (1–20). K = 10 (dashed vertical line) gives the highest average silhouette width, so was chosen as the optimum place to cut the dendrogram.

Table 3
Results of the hierarchical cluster analysis. The number of group members (ages), mean age, mean error and upper and lower quartile bounds are shown for the ten resulting groups. No interquartile range is given for Group 7 or 10 as they contain only one and two ages, respectively.

Group number	n	Mean age (ka)	1σ (ka)	Lower quartile (ka)	Upper quartile (ka)
Group 1	30	8.4	1.8	7.7	9.7
Group 2	8	39.5	6.3	35.3	44.7
Group 3	8	63.1	8.3	54.8	72
Group 4	6	87.1	4	83.6	90
Group 5	11	111.6	6	105.4	118
Group 6	16	143.8	11.8	132.5	158.8
Group 7	1	194.0	18.0	NA	NA
Group 8	8	224.1	7.2	215.5	231.3
Group 9	3	314.2	8.5	302.6	323
Group 10	2	356.2	16.2	NA	NA

The basal, interstratified sands and gravels of OM20/4 suggest a flashy flow regime from 67–62 ka, indicating deposition under arid conditions with low flow competency. MIS 4 (~ 75-60 ka) is often inferred to be very arid in southeast Arabia, due to the absence of speleothem growth recorded in Hoti Cave and the presence of dated dune sediments that have been interpreted to reflect increased dune mobility (Parker, 2010). Recording fluvial aggradation during this period is, therefore, unexpected under the IOSM model of alluvial aggradation but requires an understanding of site location and fan flow behaviour. The location of site OM20/4 in the upper part of the eastern fan-catchment system potentially means that it is more sensitive to changes in precipitation, preserving a signal of aggradation during arid MIS 4 because of the higher flow competency of wadis in their mountainous reaches, compared to downstream fans (Table 4). Significantly, the wadis that drain to the southern Batinah Coast frequently flow in their upper reaches under present climate conditions (some perennially), fed predominately by winter rainfall from the north-west. However only the largest, rare, flood events reach their distal fans (Shahin, 2007).

The basal unit of OM20/3 also dates to this period at 65.8 ± 7.6 ka (Fig. 7), although the finely laminated sediments of this unit suggest the channel may have been dammed downstream, creating a barrier to transport and creating a shallow lacustrine environment in which sediments slowly settled during deposition. Being situated at a confluence and in the steep, mountainous setting of the lower catchment feeding the Rustaq fan, it is reasonable to suggest that this could have been caused by a landslide, as recorded in the nearby catchment of Wadi Mistal (Hoffmann et al., 2015). However, it could also represent gradual overbank deposition under during higher streamflow conditions. Deposition of the upper sand unit of OM20/5 is also coeval with ages of 70–60 ka from the upper parts of the system (Fig. 7), although it displays some cross-bedding (albeit very weak) so may indicate more sustained flow. These interpretations are somewhat conflicting with the lower units of OM20/4 but may be the result of dating uncertainties or the often noisy and stochastic nature of alluvial processes. Despite this ambiguity, the ages of OM20/3/3 and OM20/5/1 were included within the cluster analysis and fall within the age cluster centred on 63.1 ka (Fig. 10). This cluster again coincides with the onset of precessional forcing at the transition from MIS 4 to 3, so these sites may represent increasing hydrological conditions. Nevertheless, the upper unit of OM20/5 being coeval with the lower units of OM20/3 and OM20/4 suggests that periods of flow did at least occasionally propagate downstream from catchments to fans at this time despite overarching regional aridity. Further work is needed to determine the signals preserved in eastern Hajar alluvial systems.

Site OM20/3 shows a sharp contact with the overlying unit of coarser fluvial sands (Table 2), suggesting an eventual increase in flow competency by ~ 45 ka (Fig. 7), with sediments continuing to coarsen upwards into overlying larger gravels and conglomerate material. Similar coarser units are observed downstream at site OM20/4 that are younger than 62 ka and can be observed along the exposed valley-fill between the two sites (Fig. 7). Multiple alluvial records from the western Hajar fans also indicate increased flow during this time (e.g. Parton et al., 2013, 2015a; Mueller et al., 2022) (Fig. 10). Marine proxies from the Arabian Sea similarly suggest enhanced monsoon precipitation, in line with precessional maxima (e.g. Clemens and Prell, 2003) (Fig. 10), as do palaeoclimate model simulations (Jennings et al., 2015). However, in the nearby Wadi Mistal catchment, Hoffmann et al. (2015) interpret alluvial sedimentation rates during MIS 3 to be similar to today's, conflicting with our record from Wadi Sahtan. The Hoti Cave speleothem also does not record growth during this period (Fleitmann et al., 2003). Ultimately, enhanced precipitation in the Hajar during MIS 3 remains debated, although our data support this hypothesis.

The upper sand unit of OM20/12 near the apex of the Dhank fan yielded an age of 25.5 ± 2.5 ka. Whilst the sedimentary interpretation for this unit is that it represents proximal floodplain deposition, this age dates to MIS 2 during precessional minima. Whilst there are other fan sediments from the region dating to this period (e.g. Mueller et al., 2022; Beuzen-Waller et al., 2022), they show sedimentary evidence for being deposited by flashy floods under more arid climate regimes. The unit fines upwards, indicating waning streamflow. Therefore, given potential dating uncertainties, this unit may represent reducing rainfall at the termination of the wetter period during Late MIS 3 (~ 30 ka).

Sites OM20/10 and/11 record aggradation in western Hajar fan systems during the Holocene (Fig. 8). An age of 6.6 ± 0.7 ka from the basal unit of OM20/11 shows the sustained flow of drainage systems. This is in agreement with numerous palaeoenvironmental records from across the region which show intensified hydrological activity during the Arabian Holocene Humid Period (AHHP), ~ 10-6 ka, such as lakes

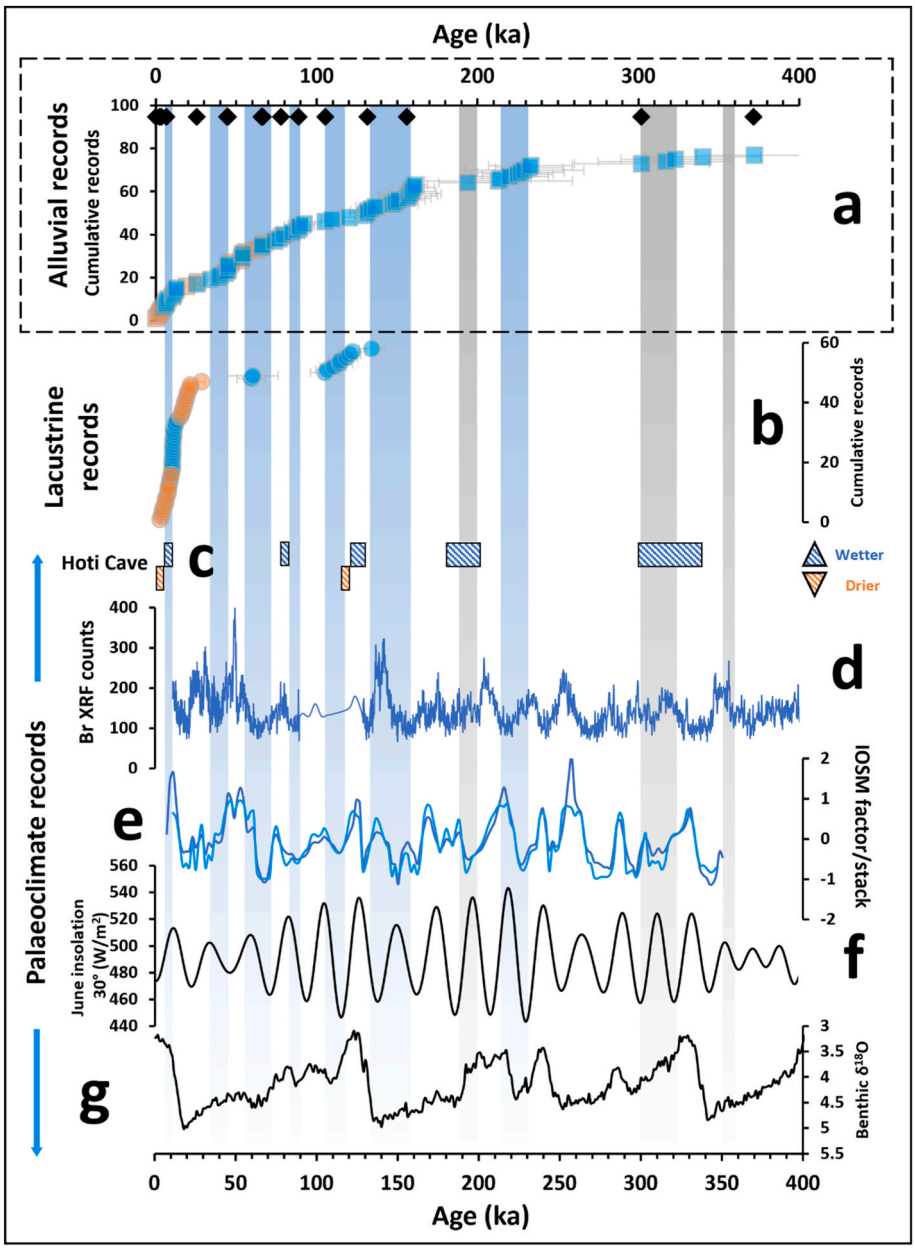

Fig. 10. Palaeoenvironmental records from the Hajar Mountains. For alluvial and lacustrine records, blue symbols denote wetter conditions relative to present and orange symbols denote similar or drier conditions to present, based on the interpretations of original authors. **a:** Alluvial records: Dalongeville (1999); Blechschmidt et al. (2009); Farrant et al. (2012); Atkinson et al. (2013); Parton et al. (2015a); Hoffmann et al. (2015); Purdue et al. (2019); Moraetis et al. (2020); Mueller et al. (2022); Beuzen-Waller et al. (2022); this study. **b:** Lacustrine records: Aqabah (Parton et al., 2013); Maqta (Fuchs and Buerkert, 2008); Wahala (Preston et al., 2015); Awafi (Parker et al., 2006); Saiwan (Rosenberg et al., 2012). Ages from this study are marked by the black diamonds. **c:** The Hoti Cave speleothem record (Fleitmann et al., 2011). Marine proxy records from the Arabian Sea: **d:** bromine XRF counts (Ziegler et al., 2010) and **e:** the IOSM factor and stack (lighter and darker blue lines, respectively; Clemens and Prell, 2003). **f:** June insolation at 30°N (Berger and Loutre, 1991). **g:** Global $\delta^{18}O$ data from the LR04 benthic stack (Lisiecki and Raymo, 2005). The vertical blue bars denote periods of intensified fan aggradation and lake sediment deposition based on the hierarchical cluster interquartile ranges (Table 3). Grey bars denote periods of intensified hydrological activity that are more speculative due to few data points (n = 1–3).

and rivers (e.g. Woor et al., 2022a), as well as speleothem and marine core records evidencing the northwards incursion of the IOSM (e.g. Sirocko et al., 1993; Clemens and Prell, 2003; Fleitmann et al., 2007) (Fig. 10). The cluster analysis suggests that fan aggradation and lake deposition intensified during this time, centred at 8.4 ka (Fig. 10). The distal setting of OM20/11 suggests that flows reached the fringes of the interior Rub'al Khali, although with reduced competency relative to more proximal locations and were likely still highly seasonal. It is unlikely that intensified IOSM precipitation directly penetrated as far inland as the distal extent of the Ibri and Dhank fans. While dune records suggest that northern and more coastal Rub'al Khali landscapes may have been stabilised (Thomas and Bailey, 2019), lacustrine records from the interior of southern Oman suggest that increased freshwater availability was the result of drainage connections with more coastal catchments and higher groundwater tables rather than direct meteoric inputs (e.g. Matter et al., 2015; Woor et al., 2022a).

The age of 3.4 ± 0.4 ka from sample OM20/11/2 indicates that flows reached the medial-distal parts of the Dhank fan later than the termination of the AHHP at ~ 6 ka (as recorded by the Hoti Cave speleothem), albeit under flashier conditions. Other fan deposits in the region have been dated to the Mid-Late Holocene, such as at Mleiha (Dalongeville, 1999) and in the Emirate of Sharjah where luminescence ages from

Table 4
Summaries of site location, luminescence age results and sedimentary interpretations for units discussed in the text.

Site	Location within system	Age (ka)	Sedimentary interpretation of flow conditions
Wadi Sahtan and the Rustaq fan			
OM20/3	Catchment	Lower unit: 66 ± 6	Shallow, ponded environment, likely the result of local damming in channel or overbank deposition. Seasonal deposition of fine sand.
		[a]Upper unit: 44.7 ± 5.1	More sustained seasonal flow within channel than at present.
OM20/4	Catchment	Lower units: 62.2 ± 7.0–66.6 ± 6.1	Flashy flow regime within channel, similar to today.
		Upper units: <62	More sustained flow regime than today with higher transport competence. Likely coeval with upper units of OM20/3.
OM20/5	Proximal fan	Lower unit: 105.4 ± 18.6	More sustained seasonal flow than today, resulting in periodic deposition onto stabilised floodplain.
		Upper unit: 66.2 ± 7.1	More sustained seasonal flow than today within channel.
Ibri and Rustaq fans			
OM20/6	Proximal fan	Lower unit: 372.5 ± 35.6 Upper unit: 302.6 ± 29.3	Greater seasonal flow than at present, resulting in deposition onto floodplains. Interstratified channel conglomerates likely date to MIS 9.
OM20/8	Medial-distal fan	Lower unit: 131.8 ± 10.7	More sustained flow regime than today. Aggradation in low energy environment of low-gradient distal fan.
		Upper unit: 88.9 ± 6.7	Perhaps similarly intermittent or slightly greater flow regime than present.
OM20/10	Medial-distal fan	Lower unit: 0.16 ± 0.04	Similar to present conditions: localised reworking of material during occasional flow events.
OM20/11	Medial-distal fan	Lower unit: 6.6 ± 0.7	More sustained flow than present in channel, resulting in development of gravel and sand bars.
		Middle unit: 3.4 ± 0.4	Potentially indicative of waning flow regimes following the southwards retreat of the IOSM rain-belt in the Mid-Late Holocene.
		Upper unit: 2.4 ± 0.3	Flashy flow regime resulting in local reworking of material, similar to present.
OM20/12	Proximal fan	Lower unit: 156.3 ± 14.9	More sustained seasonal flow within channel than today, resulting in deposition of thick conglomerate units.
		Upper unit: 255 ± 2.5	More sustained flow regime on fan relative to present.

[a] Ages and errors are averaged due to multiple ages from the same unit.

episodic flood deposits correspond with OM20/11/2 (Mueller et al., 2022).

The later Holocene ages of 2.4 ± 0.3 ka and 0.16 ± 0.04 ka from the upper unit of OM20/11 and OM20/10 (Fig. 8), respectively, have greater grain size sorting coefficients relative to those from the other fluvial deposits reported (Table 2). This could be the result of lower discharge depositing a more narrow range of grain sizes as has been observed for other dryland fluvial systems which have undergone transitions from relatively wetter to drier climates (e.g. Walsh et al., 2022a), or the local reworking of aeolian sediments which typically display a higher degree of grain size sorting than fluvial sediments (e.g. Nottebaum et al., 2014; Kapui et al., 2018). Both scenarios suggest the reduced and more localised nature of flows in the medial-distal reaches of the Dhank fan during the Late Holocene, consistent with a more arid climate depicted in regional palaeoclimate records (e.g. Clemens and Prell, 2003; Fleitmann et al., 2011) (Fig. 10). The medial distal units of western fans, therefore, indicate a switch from a more connected sediment routing system between catchments and fans to a disconnected one during the Mid-Late Holocene. At this time, sediment transport on the distal, interior bajada became dominated by aeolian processes and only occasionally moved by fluvial processes during localised rainfall events or large flash floods.

5.2. *Hajar alluvial fans as sensitive records of IOSM rainfall*

This study aims to test whether the timing of aggradation of alluvial systems in the central Hajar are paced by IOSM rainfall variability over the Late Quaternary. The periods of aggradation reported from our sites that we interpret to preserve sedimentary evidence of higher streamflow conditions relative to present largely support this model. At the regional scale, the results of the hierarchical clustering analysis show that, over the last 150 ka, aggradation periods broadly align with proxy records indicating higher IOSM rainfall in the Arabian Sea and Hoti Cave region, driven by insolation increases at precessional timescales (Berger and Loutre, 1991; Ziegler et al., 2010; Caley et al., 2011). Testing the applicability of the IOSM model is more speculative beyond ~ 150 ka, because of much poorer precision on depositional ages or an insufficient number of age-data points (Fig. 10). Despite this, age clusters still largely centre on precessional peaks overprinted on eccentricity cycles.

Blechschmidt et al. (2009) hypothesised that arid periods would likely result in increased physical weathering in Hajar mountain catchments due to intense diurnal temperature fluctuations. However, sediment supply to fans would be relatively limited due to lower seasonal rainfall. This mechanism could explain why fan aggradation is the predominate signal when IOSM rainfall increases as sediment is mobilised by an increased transport capacity. Of course, vegetation dynamics would likely play a key role in modulating this process. Vegetation may explain why aggradation periods often seem to cluster on the leading edge of precessional peaks (Fig. 10), as large amounts of sediment may be mobilised at the onset of wetter periods before the more widespread establishment of vegetation and associated lower sediment supply due to greater landscape stability. However, no long-term ecological records are currently available for the region, a common issue in arid environments (Thomas, 2013).

Whilst long-term variability in IOSM precipitation is driven by precessional cycles (e.g. Caley et al., 2011), larger scale drivers may also be important for determining rainfall and environmental conditions in south-east Arabia. Hoti Cave speleothem growth only occurs during interglacial periods at eccentricity timescales (~ 100 ka periodicity; Fleitmann et al., 2003; Lisiecki and Raymo, 2005; Fig. 10). Burns et al. (2001) suggest that warmer sea surface temperatures during interglacials would result in increased water vapour transport in Indian Ocean air masses, leading to increased precipitation. Higher IOSM rainfall during precessional maxima coinciding with Northern Hemisphere interglacial periods potentially amplified hydrological activity in alluvial systems as a result, when compared to precessional maxima that occurred during glacials (e.g. MIS 3). This may explain why fan and lacustrine ages indicative of more sustained drainage activity do not produce as discrete mean age clusters around precessional peaks from 150–100 ka (Fig. 10), relative to glacials. Therefore, interglacial conditions may have dampened the influence of precessional minima on regional rainfall during this time. The continued growth of the Hoti Cave speleothem from 120–110 ka (Fleitmann et al., 2003), following the transition from wetter MIS 5e to drier 5 d, as well as evidence of more sustained flow conditions in fan and lake systems support this hypothesis.

This hypothesis of south-east Arabian rainfall being driven by the complex overprinting of precessional and eccentricity signals may explain the discrepancies between some periods of fan aggradation and the $\delta^{18}O$ record from the Hoti Cave speleothem. Fan aggradation during

MIS 6 and 3 occurs when the Hoti Cave speleothem ceased to grow (Fleitmann et al., 2003) (Fig. 10). Previous authors have suggested that this discrepancy could be because alluvial systems in the Hajar have a lower threshold for aggradation relative to speleothem growth. The Hoti Cave speleothem requires >300–350 mm of rainfall for stalagmites to form (Vaks et al., 2006; Fleitmann et al., 2011; Parton et al., 2015a; Nicholson et al., 2020). Modern observations of wadi flow in the mountainous catchments of the Hajar support the idea that streamflow occurrence has a lower precipitation threshold, with seasonal flows occurring under present mean annual rainfall levels of 142.6 mm yr^{-1} for the Hajar Mountains (Shahin, 2007; Kwarteng et al., 2009), half of the >300–350 mm threshold required for speleothem growth. Therefore, even small increases in regional rainfall are more likely to result in alluvial aggradation, as occur with precessional peaks during glacials, relative to the larger increases in rainfall when precessional peaks coincide with interglacials and rainfall becomes sufficient for speleothem growth to occur.

The sensitivity of regional drainage networks to small increases of rainfall is further evidenced by an increasing number of fan and valley-fill deposits dated to periods when the IOSM model predicts very limited fan aggradation, such as the sediments from Wadi Sahtan dating to MIS 4 (Table 4). Fluvial deposits from drier periods have also recently been dated to ~ 20 ka and the Late Holocene (0–3 ka) in the UAE (Mueller et al., 2022). However, the sedimentary interpretations of both Mueller et al. (2022) and many of the horizons dating to this period in this study suggest that these sediments were deposited by more intermittent flows than the bedded, coarser materials typically observed in association with periods of more intense IOSM rainfall. These deposits possibly represent similar low-frequency, high-magnitude events to those which occur across the Hajar region today (Kwarteng et al., 2009), with flows only periodically having sufficient energy to transmit sediment out of mountainous catchments to distal fan systems. As such, careful interpretation must be made of these deposits in terms of the hydrological signal they preserve.

The sites sampled in Wadi Sahtan are also all located within the mountainous setting of a fan-feeding catchment. Numerous ages assembled in the Synthesising Chronologies of Arabian PalaeoEnvironments (SCAPE) database from catchment settings in the Hajar show similarly 'anomalous' hydrological activity, relative to established periods of greater regional precipitation, in fluvial systems (Woor et al., 2022a). For example, the Maqta basin in the southern-central Hajar records deposition almost continually over the last 20 ka, except for a hiatus from ~ 12–10.5 ka, as well as Wadi Dishshah in the southern Hajar recording sedimentation at ~ 26 ka (Beuzen-Waller et al., 2022). However, these ages at odds with the IOSM model are to be expected in mountainous settings due to the higher likelihood of flow occurrence in the steeper, elevated uplands of the Hajar. These are unlikely to transmit sediment further downstream in the system under periods of regionally more arid climate such as today (Shahin, 2007). Outside of the largest flash flood events, flows only have the sustained competence to contribute significant sediment loads downstream beyond mountain fronts during the wettest regional conditions.

5.3. Resolution and scale

We have already commented on the limited spatial coverage of previously published records from alluvial settings in the Hajar. Sampling is also biased by the inherent spatial heterogeneity of large fan systems where active channels tend to incise through relict, inactive surfaces and avulse across the fan over time (Bryant et al., 1995). As such, the temporal signals preserved by fans will be spatially heterogeneous. This is evidenced in this study: for example, we record no deposition at the sites sampled from ~ 220-230 ka which other studies have shown to be a key period of Hajar fan aggradation (e.g. Blechschmidt et al., 2009). Contrastingly, the al Sibetah fan (Parton et al., 2015a) records no Early-Mid Holocene aggradation, which has also been established as a key period of regional fan aggradation. This does not necessarily mean that these systems did not respond to these periods of increased intensity and northwards displacement of the IOSM, but rather building a complete picture of Late Quaternary responses is difficult with spatially complex deposits. Taking a multi-site approach to sampling fan deposits as well as amalgamating data from similar depositional settings, as adopted in this study, is potentially means for resolving this issue.

In addition to spatial resolution and scale, considering temporal resolution with regards to this discussion is also important. The precision of OSL dating is usually ~ ±10% (Mejdahl and Christiansen, 1994; excluding the very young age of OM20/10/3, the mean relative uncertainty of ages in this study is ±10.7%; Table 1). Therefore, environmental changes at ~ 23 ka periodicity can only be clearly distinguished over approximately the last 100–120 ka, beyond which the precision limits on OSL dating make drawing conclusions between cause and effect more difficult. Similarly, more rapid environmental and climatic changes at sub-orbital timescales are also difficult to resolve within current precision limits, yet rapid drying associated with the 8.2 ka and 4.2 ka events are resolved by radiocarbon dating in lacustrine records from the north-western Hajar (Parker et al., 2016). Despite these challenges, the OSL dating and stratigraphic interpretations of alluvial sediments in the Hajar provide an important long-term environmental record for a region where other proxies are limited.

6. Conclusions

The alluvial fans of the Hajar Mountains, south-east Arabia, are the most spatially and temporally extensive geomorphological records of the region's palaeoenvironmental and palaeohydrological variability over the last 400 ka. Through our wide spatial sampling of alluvial sediments both east and west of the Hajar Mountains and the use of hierarchical clustering to synthesise these data with other sites across the region, we record periods of more sustained flow and fan aggradation occurring at precessional timescales. These main aggradation phases are driven by the northwards displacement of the IOSM and build an increasingly comprehensive picture of precessionally-paced fan aggradation throughout the Late Quaternary in response to climate variability. However, the signals preserved by Hajar fans are still noisy and, in some circumstances, conflicting. For instance, we find further evidence of greater hydrological activity during MIS 3, relative to today, which agrees with the findings of some authors (e.g. Farrant et al., 2012), whilst disagreeing with the interpretations of others (e.g. Hoffmann et al., 2015).

Additionally, we also find evidence of palaeohydrological activity and deposition not solely occurring in these periods of increased rainfall, relative to the present. Fluvial deposits dating to the Late Holocene and MIS 4 represent apparent anomalies in this framework of the IOSM model of fan aggradation, occurring during more arid periods in south-east Arabia. Present aridity does not entirely preclude the region's wadi systems from flowing, with episodic flooding or seasonal flows in response to winter rainfall being commonplace, especially in catchment settings. Therefore, we attribute these seemingly anomalous ages to similar types of activity in the past: it does rain in deserts during arid periods and sediment does move through fluvial systems when this occurs.

The resulting interpretation is one of mountain catchments that retain a certain degree of flow activity through periods of broad regional aridity, with occasional high-magnitude, low-frequency events connecting fans and catchments or causing the localised reworking of sediments. Overprinted on this are signals preserved from periods of precessionally-paced increases in the intensity of the IOSM and its northwards displacement, resulting in more sustained periods of flow, higher stream competency and significant fan aggradation which is amplified during eccentricity-paced interglacial periods. Hierarchical clustering shows that periods of fan and lake sediment deposition from

the region occurs centred on the onsets or peaks of precessional forcing, and is also likely intensified by global interglacial conditions.

There is a growing awareness of the nuances of the palaeoenvironmental signals preserved in a variety of geomorphological, isotopic and biological proxies across south-east Arabia that move beyond an overly simplistic narrative of the region being either 'wet' or 'dry' (Petraglia et al., 2020; Woor et al., 2022a; Mueller et al., 2022; Beuzen-Waller et al., 2022). The alluvial sediments of the Hajar Mountains paint an increasingly complex picture of landscape responses to Mid-Late Quaternary climate variability, as well as having important implications for an increasingly complex archaeological record of hominin occupation in the region (e.g. Bretzke et al., 2022).

Author contributions

SW, DT, AP, JD and SB conceived the project. Fieldwork was undertaken by SW, DT and AP. SW conducted all sample preparation, laboratory and formal data analyses under the guidance of JD and SB. SW constructed all figures. The original draft of the manuscript and its revisions were drafted by SW and then reviewed and edited by DT, JD and SB.

Declaration of competing interest

The authors have no conflicts of interest to declare.

Data availability

Data is available in the Supplementary Information files attached to this article.

Acknowledgements

This work was supported by the UK's Engineering and Physical Sciences Research Council (EPSRC) grant for the Centre for Doctoral Training: Science and Engineering in Art, Heritage and Archaeology (SEAHA) (EP/L016036/1). Fieldwork was undertaken thanks to the permissions granted by the Oman Ministry of Heritage and Culture. SW, DT and AP would like to thank Professor Simon Underdown for funding part of the fieldwork through the Beatrice de Cardi Award from the Society of Antiquaries and for his, and Dr Sam Smith's, assistance in the field. The authors would like to thank Prof. Tony Reimann and one anonymous reviewer for their insightful comments that greatly improved this manuscript.

Appendix A. Supplementary data

Supplementary data to this article can be found online at https://doi.org/10.1016/j.quascirev.2023.108384.

References

Abrams, M., Chadwick, O., 1994. Tectonic and climatic implications of alluvial fan sequences along the Batinah coast, Oman. J. Geol. Soc. 151, 51–58.
Al-Farraj, A., Harvey, A.M., 2000. Desert pavement characteristics on wadi terrace and alluvial fan surfaces: wadi Al-Bih, UAE and Oman. Geomorphology 35, 279–297.
Al-Farraj, A., Harvey, A.M., 2005. Morphometry and depositional style of Late Pleistocene alluvial fans: wadi Al-Bih, northern UAE and Oman. Geological Society, London, Special Publications 251, 85–94.
Al Farraj, A., Harvey, A.M., 2004. Late Quaternary interactions between aeolian and fluvial processes: a case study in the northern UAE. J. Arid Environ. 56, 235–248.
Ali, M., Aidarbayev, S., Searle, M., Watts, A., 2018. Subsidence history and seismic stratigraphy of the western Musandam Peninsula, Oman–United Arab Emirates mountains. Tectonics 37, 154–181.
Arnold, L.J., Bailey, R.M., Tucker, G.E., 2007. Statistical treatment of fluvial dose distributions from southern Colorado arroyo deposits. Quat. Geochronol. 2 (1–4), 162–167.
Atkinson, O.A., Thomas, D.S., Goudie, A.S., Bailey, R.M., 2011. Late Quaternary chronology of major dune ridge development in the northeast Rub'al-Khali, United Arab Emirates. Quat. Res. 76, 93–105.
Atkinson, O.A., Thomas, D.S., Parker, A.G., Goudie, A.S., 2013. Late Quaternary humidity and aridity dynamics in the northeast Rub'al-Khali, United Arab Emirates: implications for early human dispersal and occupation of eastern Arabia. Quat. Int. 300, 292–301.
Bartz, M., Walk, J., Binnie, S.A., Brill, D., Stauch, G., Lehmkuhl, F., Hoffmeister, D., Brueckner, H., 2020. Late Pleistocene alluvial fan evolution along the coastal Atacama Desert (N Chile). Global Planet. Change 190, 103091.
Bell, W., 1979. Attenuation factors for the absorbed radiation dose in quartz inclusions for thermoluminescence dating. Ancient TL 8, 12.
Berger, A., Loutre, M.-F., 1991. Insolation values for the climate of the last 10 million years. Quat. Sci. Rev. 10, 297–317.
Beuzen-Waller, T., Desruelles, S., Marrast, A., Giraud, J., Gernez, G., Forman, S., Beshkani, A., Bonilauri, S., Lemée, M., Nacarro, H., 2022. Late pleistocene-holocene fluvial records of the wadi Dishshah: hydro-climatic and archaeological implications (southern piedmont of the hajar mountains, Oman). Géomorphol. Relief, Process. Environ. 28 (4).
Blair, T.C., Mcpherson, J.G., 1994. Alluvial fans and their natural distinction from rivers based on morphology, hydraulic processes, sedimentary processes, and facies assemblages. J. Sediment. Res. 64, 450–489.
Blechschmidt, I., Matter, A., Preusser, F., Rieke-Zapp, D., 2009. Monsoon triggered formation of Quaternary alluvial megafans in the interior of Oman. Geomorphology 110, 128–139.
Blott, S.J., Pye, K., 2001. GRADISTAT: a grain size distribution and statistics package for the analysis of unconsolidated sediments. Earth Surf. Process. Landforms 26, 1237–1248.
Bowman, D., 2019. Principles of Alluvial Fan Morphology. Springer.
Bretzke, K., Parton, A., Lindauer, S., Kennet, D., 2018. Evidence of neolithic settlement in the foothills of the western al-hajar mountains. Arabian Archaeol. Epigr. 29, 103–114.
Bretzke, K., Preusser, F., Jasim, S., Miller, C., Preston, G., Raith, K., Underdown, S., Parton, A., Parker, A., 2022. Multiple phases of human occupation in Southeast Arabia between 210,000 and 120,000 years ago. Sci. Rep. 12, 1–9.
Bryant, M., Falk, P., Paola, C., 1995. Experimental study of avulsion frequency and rate of deposition. Geology 23, 365–368.
Burns, S.J., Fleitmann, D., Matter, A., Neff, U., Mangini, A., 2001. Speleothem evidence from Oman for continental pluvial events during interglacial periods. Geology 29, 623–626.
Burns, S.J., Matter, A., Frank, N., Mangini, A., 1998. Speleothem-based paleoclimate record from northern Oman. Geology 26, 499–502.
Caley, T., Malaizé, B., Zaragosi, S., Rossignol, L., Bourget, J., Eynaud, F., Martinez, P., Giraudeau, J., Charlier, K., Ellouz-Zimmermann, N., 2011. New Arabian Sea records help decipher orbital timing of Indo-Asian monsoon. Earth Planet Sci. Lett. 308, 433–444.
Clemens, S.C., Prell, W.L., 2003. A 350,000 year summer-monsoon multi-proxy stack from the owen ridge, northern Arabian Sea. Mar. Geol. 201, 35–51.
Corradetti, A., Spina, V., Tavani, S., Ringenbach, J.-C., Sabbatino, M., Razin, P., Laurent, O., Brichau, S., Mazzoli, S., 2020. Late-stage tectonic evolution of the Al-Hajar Mountains, Oman: new constraints from Palaeogene sedimentary units and low-temperature thermochronometry. Geol. Mag. 157, 1031–1044.
Dalongeville, R., 1999. Mleiha: étude physique et paléoenvironnement. MOM Éditions 29, 33–54.
D'Arcy, M., Whittaker, A.C., 2014. Geomorphic constraints on landscape sensitivity to climate in tectonically active areas. Geomorphology 204, 366–381.
D'Arcy, M., Roda-Boluda, D.C., Whittaker, A.C., 2017. Glacial-interglacial climate changes recorded by debris flow fan deposits, Owens Valley, California. Quat. Sci. Rev. 169, 288–311.
Duller, G., 2003. Distinguishing quartz and feldspar in single grain luminescence measurements. Radiat. Meas. 37, 161–165.
Durcan, J.A., Duller, G.A., 2011. The fast ratio: a rapid measure for testing the dominance of the fast component in the initial OSL signal from quartz. Radiat. Meas. 46, 1065–1072.
Durcan, J.A., King, G.E., Duller, G.A., 2015. DRAC: dose rate and age calculator for trapped charge dating. Quat. Geochronol. 28, 54–61.
Durcan, J.A., Thomas, D.S., Gupta, S., Pawar, V., Singh, R.N., Petrie, C.A., 2019. Holocene landscape dynamics in the Ghaggar-Hakra palaeochannel region at the northern edge of the Thar Desert, northwest India. Quat. Int. 501, 317–327.
Farrant, A., Ellison, R., Thomas, R., Pharaoh, T., Newell, A., Goodenough, K., Lee, J., Knox, R., 2012. The geology and geophysics of the United Arab Emirates. Volume 6, geology of the western and central United Arab Emirates, 336pp. British Geological Survey.
Fick, S.E., Hijmans, R.J., 2017. WorldClim 2: new 1-km spatial resolution climate surfaces for global land areas. Int. J. Climatol. 37, 4302–4315.
Fleitmann, D., Burns, S.J., Mangini, A., Mudelsee, M., Kramers, J., Villa, I., Neff, U., Al-Subbary, A.A., Buettner, A., Hippler, D., 2007. Holocene ITCZ and Indian monsoon dynamics recorded in stalagmites from Oman and Yemen (Socotra). Quat. Sci. Rev. 26, 170–188.
Fleitmann, D., Burns, S.J., Neff, U., Mangini, A., Matter, A., 2003. Changing moisture sources over the last 330,000 years in Northern Oman from fluid-inclusion evidence in speleothems. Quat. Res. 60, 223–232.
Fleitmann, D., Burns, S.J., Pekala, M., Mangini, A., Al-Subbary, A., Al-Aowah, M., Kramers, J., Matter, A., 2011. Holocene and Pleistocene pluvial periods in Yemen, southern Arabia. Quat. Sci. Rev. 30, 783–787.
Fleitmann, D., Matter, A., 2009. The speleothem record of climate variability in Southern Arabia. Compt. Rendus Geosci. 341, 633–642.

Fuchs, M., Buerkert, A., 2008. A 20 ka sediment record from the Hajar Mountain range in N-Oman, and its implication for detecting arid–humid periods on the southeastern Arabian Peninsula. Earth Planet Sci. Lett. 265, 546–558.
Galbraith, R.F., Laslett, G.M., 1993. Statistical models for mixed fission track ages. Nucl. Tracks Radiat. Meas. 21, 459–470.
Galbraith, R.F., Roberts, R.G., Laslett, G.M., Yoshida, H., Olley, J.M., 1999. Optical dating of single and multiple grains of quartz from Jinmium rock shelter, northern Australia: Part I, experimental design and statistical models. Archaeometry 41, 339–364.
Galbraith, R.F., Roberts, R.G., 2012. Statistical aspects of equivalent dose and error calculation and display in OSL dating: an overview and some recommendations. Quat. Geochronol. 11, 1–27.
Glennie, K., Boeuf, M., Clarke, M.H., Moody-Stuart, M., Pilaar, W., Reinhardt, B., 1973. Late Cretaceous nappes in Oman Mountains and their geologic evolution. AAPG (Am. Assoc. Pet. Geol.) Bull. 57, 5–27.
Guérin, G., Jain, M., Thomsen, K.J., Murray, A.S., Mercier, N., 2015. Modelling dose rate to single grains of quartz in well-sorted sand samples: the dispersion arising from the presence of potassium feldspars and implications for single grain OSL dating. Quat. Geochronol. 27, 52–65.
Guérin, G., Mercier, N., Nathan, R., Adamiec, G., Lefrais, Y., 2012. On the use of the infinite matrix assumption and associated concepts: a critical review. Radiat. Meas. 47, 778–785.
Guérin, G., Christophe, C., Philippe, A., Murray, A.S., Thomsen, K.J., Tribolo, C., Urbanová, P., Jain, M., Guibert, P., Mercier, N., Kreutzer, S., 2017. Absorbed dose, equivalent dose, measured dose rates, and implications for OSL age estimates: introducing the Average Dose Model. Quat. Geochronol. 41, 163–173.
Guilmette, C., Smit, M.A., Van Hinsbergen, D.J., Gürer, D., Corfu, F., Charette, B., Maffione, M., Rabeau, O., Savard, D., 2018. Forced subduction initiation recorded in the sole and crust of the Semail Ophiolite of Oman. Nat. Geosci. 11, 688–695.
Hartley, A.J., Weissmann, G.S., Nichols, G.J., Warwick, G.L., 2010. Large distributive fluvial systems: characteristics, distribution, and controls on development. J. Sediment. Res. 80 (2), 167–183.
Harvey, A., 2011. Dryland alluvial fans. In: Thomas, D. (Ed.), Arid Zone Geomorphology: Process, Form and Change in Drylands.
Hoffmann, G., Rupprechter, M., Rahn, M., Preusser, F., 2015. Fluvio-lacustrine deposits reveal precipitation pattern in SE Arabia during early MIS 3. Quat. Int. 382, 145–153.
Hoffmann, G., Schneider, B., Mechernich, S., Falkenroth, M., Dunai, T., Preusser, F., 2020. Quaternary uplift along a passive continental margin (Oman, Indian Ocean). Geomorphology 350, 106870.
Jain, M., Murray, A.S., Botter-Jensen, L., 2004. Optically stimulated luminescence dating: how significant is incomplete light exposure in fluvial environments? [Datation par luminescence stimulée optiquement: quelle significant en cas de blanchiment incomplet des sédiments fluviatiles?]. Quaternaire 15 (1), 143–157.
Jennings, R.P., Singarayer, J., Stone, E.J., Krebs-Kanzow, U., Khon, V., Nisancioglu, K.H., Pfeiffer, M., Zhang, X., Parker, A., Parton, A., 2015. The greening of Arabia: multiple opportunities for human occupation of the Arabian Peninsula during the Late Pleistocene inferred from an ensemble of climate model simulations. Quat. Int. 382, 181–199.
Kalińska, E., Weckwerth, P., Alexanderson, H., 2022. Recent advances in luminescence dating of the late quaternary sediments in the baltic states, northern europe: a review. Earth Sci. Rev., 104272
Kapui, Z., Kereszturi, A., Kiss, K., Szalai, Z., Újvári, G., Hickman-Lewis, K., Foucher, F., Westall, F., 2018. Fluvial or aeolian grains? Separation of transport agents on Mars using earth analogue observations. Planet. Space Sci. 163, 56–76.
Kenworthy, M., Rittenour, T.M., Pierce, J.L., Sutfin, N.A., Sharp, W.D., 2014. Luminescence dating without sand lenses: an application of OSL to coarse-grained alluvial fan deposits of the Lost River Range, Idaho, USA. Quat. Geochronol. 23, 9–25.
Kreutzer, S., Schmidt, C., Fuchs, M.C., Dietze, M., Fischer, M., Fuchs, M., 2012. Introducing an R package for luminescence dating analysis. Ancient TL 30 (1), 1–8.
Kusky, T., Robinson, C., El-Baz, F., 2005. Tertiary–quaternary faulting and uplift in the northern Oman hajar mountains. J. Geol. Soc. 162, 871–888.
Kwarteng, A.Y., Dorvlo, A.S., Vijaya Kumar, G.T., 2009. Analysis of a 27-year rainfall data (1977–2003) in the Sultanate of Oman. Int. J. Climatol.: A Journal of the Royal Meteorological Society 29, 605–617.
Lecce, S.A., 1990. The alluvial fan problem. In: Alluvial Fans: A Field Approach, pp. 3–24.
Lisiecki, L.E., Raymo, M.E., 2005. A Pliocene-Pleistocene stack of 57 globally distributed benthic δ18O records. Paleoceanography 20.
Maizels, J., 1987. Plio-Pleistocene raised channel systems of the western Sharqiya (Wahiba), Oman. Geological Society, London, Special Publications 35, 31–50.
Maizels, J., 1990. Raised channel systems as indicators of palaeohydrologic change: a case study from Oman. Palaeogeogr. Palaeoclimatol. Palaeoecol. 76, 241–277.
Maizels, J., Mcbean, C., 1990. Cenozoic alluvial fan systems of interior Oman: palaeoenvironmental reconstruction based on discrimination of palaeochannels using remotely sensed data. Geological Society, London, Special Publications 49, 565–582.
Matter, A., Neubert, E., Preusser, F., Rosenberg, T., Al-Wagdani, K., 2015. Palaeo-environmental implications derived from lake and sabkha deposits of the southern Rub'al-Khali, Saudi Arabia and Oman. Quat. Int. 382, 120–131.
Mayya, Y., Morthekai, P., Murari, M.K., Singhvi, A., 2006. Towards quantifying beta microdosimetric effects in single-grain quartz dose distribution. Radiat. Meas. 41, 1032–1039.
Mejdahl, V., Christiansen, H.H., 1994. Procedures used for luminescence dating of sediments. Quat. Sci. Rev. 13, 403–406.
Miall, A.D., 1977. Lithofacies Types and Vertical Profile Models in Braided River Deposits: a Summary.
Moraetis, D., Scharf, A., Mattern, F., Pavlopoulos, K., Forman, S., 2020. Quaternary Thrusting in the central Oman Mountains—novel observations and causes: insights from optical stimulate luminescence dating and kinematic fault analyses. Geosciences 10, 166.
Moscariello, A., 2018. Alluvial fans and fluvial fans at the margins of continental sedimentary basins: geomorphic and sedimentological distinction for geo-energy exploration and development. Geological Society, London, Special Publications 440, 215–243.
Mueller, D., Raith, K., Bretzke, K., Fülling, A., Parker, A.G., Parton, A., Preston, G.W., Jasim, S., Yousif, E., Preusser, F., 2022. Luminescence chronology of fluvial and aeolian deposits from the Emirate of Sharjah, UAE. Quat. Res. 1–17.
Murray, A.S., Wintle, A.G., 2003. The single aliquot regenerative dose protocol: potential for improvements in reliability. Radiat. Meas. 37, 377–381.
Nathan, R., Mauz, B., 2008. On the dose-rate estimate of carbonate-rich sediments for trapped charge dating. Radiat. Meas. 43, 14–25.
Nathan, R.P., Thomas, P.J., Jain, M., Murray, A.S., Rhodes, E.J., 2003. Environmental dose rate heterogeneity of beta radiation and its implications for luminescence dating: Monte Carlo modelling and experimental validation. Radiat. Meas. 37, 305–313.
Nicholson, S.L., Pike, A.W., Hosfield, R., Roberts, N., Sahy, D., Woodhead, J., Cheng, H., Edwards, R.L., Affolter, S., Leuenberger, M., 2020. Pluvial periods in Southern Arabia over the last 1.1 million-years. Quat. Sci. Rev. 229, 106112.
Nottebaum, V., Lehmkuhl, F., Stauch, G., Hartmann, K., Wünnemann, B., Schimpf, S., Lu, H., 2014. Regional grain size variations in aeolian sediments along the transition between Tibetan highlands and north-western Chinese deserts–the influence of geomorphological settings on aeolian transport pathways. Earth Surf. Process. Landforms 39, 1960–1978.
Overpeck, J., Anderson, D., Trumbore, S., Prell, W., 1996. The southwest Indian Monsoon over the last 18 000 years. Clim. Dynam. 12, 213–225.
Parker, A.G., 2010. Pleistocene climate change in Arabia: developing a framework for hominin dispersal over the last 350 ka. In: The Evolution of Human Populations in Arabia. Springer.
Parker, A.G., Goudie, A.S., Stokes, S., White, K., Hodson, M.J., Manning, M., Kennet, D., 2006. A record of Holocene climate change from lake geochemical analyses in southeastern Arabia. Quat. Res. 66, 465–476.
Parker, A.G., Preston, G.W., Parton, A., Walkington, H., Jardine, P.E., Leng, M.J., Hodson, M.J., 2016. Low-latitude Holocene hydroclimate derived from lake sediment flux and geochemistry. J. Quat. Sci. 31, 286–299.
Parton, A., Bretzke, K., 2020. The PalaeoEnvironments and ARchaeological landscapes (PEARL) project: recent findings from neolithic sites in northern Oman. Arabian Archaeol. Epigr. 31, 194–201.
Parton, A., Farrant, A.R., Leng, M.J., Schwenninger, J.-L., Rose, J.I., Uerpmann, H.-P., Parker, A.G., 2013. An early MIS 3 pluvial phase in Southeast Arabia: climatic and archaeological implications. Quat. Int. 300, 62–74.
Parton, A., White, T.S., Parker, A.G., Breeze, P.S., Jennings, R., Groucutt, H.S., Petraglia, M.D., 2015a. Orbital-scale climate variability in Arabia as a potential motor for human dispersals. Quat. Int. 382, 82–97.
Parton, A., Farrant, A.R., Leng, M.J., Telfer, M.W., Groucutt, H.S., Petraglia, M.D., Parker, A.G., 2015b. Alluvial fan records from southeast Arabia reveal multiple windows for human dispersal. Geology 43, 295–298.
Preston, G.W., Thomas, D.S., Goudie, A.S., Atkinson, O.A., Leng, M.J., Hodson, M.J., Walkington, H., Charpentier, V., Méry, S., Borgi, F., 2015. A multi-proxy analysis of the Holocene humid phase from the United Arab Emirates and its implications for southeast Arabia's Neolithic populations. Quat. Int. 382, 277–292.
Preusser, F., Radies, D., Matter, A., 2002. A 160,000-year record of dune development and atmospheric circulation in southern Arabia. Science 296, 2018–2020.
Purdue, L., Charbonnier, J., Regagnon, E., Calastrenc, C., Sagory, T., Virmoux, C., Crépy, M., Costa, S., Benoist, A., 2019. Geoarchaeology of Holocene oasis formation, hydro-agricultural management and climate change in Masafi, southeast Arabia (UAE). Quat. Res. 92, 109–132.
Rhodes, E., Schwenninger, J., 2007. Dose rates and radioisotope concentrations in the concrete calibration blocks at Oxford. Ancient TL 25, 5–8.
Rittenour, T.M., 2008. Luminescence dating of fluvial deposits: applications to geomorphic, palaeoseismic and archaeological research. Boreas 37, 613–635.
Rodgers, D.W., Gunatilaka, A., 2003. Bajada formation by monsoonal erosion of a subaerial forebulge, Sultanate of Oman. Sediment. Geol. 154, 127–146.
Rodnight, H., Duller, G., Wintle, A., Tooth, S., 2006. Assessing the reproducibility and accuracy of optical dating of fluvial deposits. Quat. Geochronol. 1, 109–120.
Rosenberg, T.M., Preusser, F., Blechschmidt, I., Fleitmann, D., Jagher, R., Matter, A., 2012. Late Pleistocene palaeolake in the interior of Oman: a potential key area for the dispersal of anatomically modern humans out-of-Africa? J. Quat. Sci. 27, 13–16.
Rousseau, M., Dromart, G., Garcia, J.-P., Atrops, F., Guillocheau, F., 2005. Jurassic evolution of the Arabian carbonate platform edge in the central Oman Mountains. J. Geol. Soc. 162, 349–362.
Rousseeuw, P.J., 1987. Silhouettes: a graphical aid to the interpretation and validation of cluster analysis. J. Comput. Appl. Math. 20, 53–65.
Savi, S., Tofelde, S., Wickert, A.D., Bufe, A., Schildgen, T.F., Strecker, M.R., 2020. Interactions between main channels and tributary alluvial fans: channel adjustments and sediment-signal propagation. Earth Surf. Dyn. 8 (2), 303–322.
Schildgen, T., Tofelde, S., D'Arcy, M., Wickert, A., 2019. Alluvial system records of climate forcing and their impact on depositional sinks. In: Geophysical Research Abstracts, vol. 21.
Shahin, M., 2007. Wadis and wadi flow. In: Water Resources and Hydrometeorology of the Arab Region. Springer.

Sirocko, F., Sarnthein, M., Erlenkeuser, H., Lange, H., Arnold, M., Duplessy, J.C., 1993. Century-scale events in monsoonal climate over the past 24,000 years. Nature 364, 322–324.
Terrizzano, C.M., Morabito, E.G., Christl, M., Likerman, J., Tobal, J., Yamin, M., Zech, R., 2017. Climatic and tectonic forcing on alluvial fans in the southern central andes. Quat. Sci. Rev. 172, 131–141.
Terry, J., Al Ruheili, A., Boldi, R., Gienko, G., Stahl, H., 2022. Cyclone shaheen: the exceptional tropical cyclone of october 2021 in the gulf of Oman. Weather 77, 364–370.
Thomas, D.S., Bailey, R.M., 2019. Analysis of late Quaternary dunefield development in Asia using the accumulation intensity model. Aeolian Research 39, 33–46.
Thomas, D.S., Burrough, S.L., 2012. Interpreting geoproxies of late Quaternary climate change in African drylands: implications for understanding environmental change and early human behaviour. Quat. Int. 253, 5–17.
Thomas, D.S.G., 2013. Reconstructing paleoenvironments and palaeoclimates in drylands: what can landform analysis contribute? Earth Surf. Process. Landforms 38, 3–16.
Vaks, A., Bar-Matthews, M., Ayalon, A., Matthews, A., Frumkin, A., Dayan, U., Halicz, L., Almogi-Labin, A., Schilman, B., 2006. Paleoclimate and location of the border between Mediterranean climate region and the Saharo–Arabian Desert as revealed by speleothems from the northern Negev Desert, Israel. Earth Planet Sci. Lett. 249, 384–399.
Walsh, E., Caracciolo, L., Ravidà, D., Burrough, S., Thomas, D., 2022a. Holocene fluvial depositional regimes of the huab river, skeleton coast, Namibia. Earth Surf. Process. Landforms 47, 1820–1844.
Walsh, E.V., Burrough, S.L., Thomas, D.S., 2022b. A chronological database assessing the late Quaternary palaeoenvironmental record from fluvial sediments in southwestern Africa. Earth Sci. Rev., 104288
Whittaker, A.C., 2012. How do landscapes record tectonics and climate? Lithosphere 4 (2), 160–164.
Wintle, A.G., Murray, A.S., 2006. A review of quartz optically stimulated luminescence characteristics and their relevance in single-aliquot regeneration dating protocols. Radiat. Meas. 41, 369–391.
Woor, S., Buckland, C., Parton, A., Thomas, D.S., 2022a. Assessing the robustness of geochronological records from the Arabian Peninsula: a new synthesis of the last 20 ka. Global Planet. Change, 103748.
Woor, S., Durcan, J.A., Burrough, S.L., Parton, A., Thomas, D.S., 2022b. Evaluating the effectiveness of heavy liquid density separation in isolating K-feldspar grains using alluvial sediments from the Hajar Mountains, Oman. Quat. Geochronol. 72, 101368.
Woor, S., Thomas, D.S., Parton, A., Leenman, A., 2023. Morphology and controls of the mountain front fan systems of the Hajar Mountains, south-east Arabia. Earth Sci. Rev., 104316
Ziegler, M., Lourens, L.J., Tuenter, E., Hilgen, F., Reichart, G.-J., Weber, N., 2010. Precession phasing offset between Indian summer monsoon and Arabian Sea productivity linked to changes in Atlantic overturning circulation. Paleoceanography 25 n/a-n/a.